Characterizing particulate carbon using dielectric property measurements

Madeleine Syk
Joakim Vollmer

UPPSALA
UNIVERSITET

ABSTRACT

Interest in effects of carbonaceous particles in the atmosphere has recently taken an upswing due to knowledge of how these particles affect our environment. Carbonaceous aerosols are characterized by their dark color, giving them the ability to absorb both incoming and outgoing radiation of all wavelengths in the atmosphere. If these particles are deposited on snow or ice they blacken the surface, with an increased rate of melting as a consequence. These particles play a significant role in climate change and it is important to characterize the particles in order to determine their environmental impact and their origin. In this thesis, two non-destructive dielectric measurement approaches for characterizing carbonaceous particles at microwave frequencies were explored: measurements with an impedance analyzer and measurements using a cavity resonator. Measurements were carried out on quartz filters containing concentrations of carbon normally found in snow in northern Scandinavia. To validate the carbon concentration on the filters a field trip to northern Sweden was conducted. Snow samples were collected and analyzed in regards of carbon content, confirming that the amount of carbon on the filters were accurate. The impedance analyzer showed great uncertainty and the results were not precise enough to determine the credibility of the approach. Measurements with the cavity resonator showed some promising results due to its extreme sensitivity but require adjustments to distinguish different particle types from each other. Thus, it is expected that the use of a cavity resonator operating at microwave frequencies will become an applicable method for characterizing carbonaceous particles in the future.

REFERAT

Intresset för de effekter mörka kolhaltiga sotpartiklar har på vår atmosfär har på senaste tiden växt sig allt större. Den mörka färgen innebär att både inkommande och utgående strålning absorberas av partiklarna, och i utbyte avges värme till atmosfären. I de fall där kolpartiklarna deponeras på snö- eller istäcken mörkläggs dessa annars vita ytor. Det leder till en ökad smälttakt av de snö- och islager som finns på jorden. Det innebär att dessa partiklar innehar en viktig roll gällande den globala uppvärmningen. Eftersom utsläppen av dessa luftburna partiklar är svåra att kontrollera och partiklarna kan färdas långt i atmosfären är det viktigt att karakterisera partiklarna för att kunna bestämma deras miljöpåverkan och ursprung. De metoder som idag används för att identifiera dessa kolpartiklar kräver både tid och avancerad mätutrustning.

I det här projektet har två metoder, för att karakterisera olika typer av kolpartiklar, analyserats. Metoderna har gemensamt att mätningar av partiklarnas dielektriska egenskaper utförs då de utsätts för mikrovågor. Beroende på metod utfördes mätningarna antingen med en impedansanalysator eller en vågledare. Mätproverna bestod av kvartsfilter innehållande kolkoncentrationer typiska för snö i norra Skandinavien. Resultaten från impedansanalysatorn uppvisade mycket stor osäkerhet och var därför inte tillräckliga för att kunna bedöma trovärdigheten hos metoden. Försöken med vågledaren uppvisade inte heller önskvärda resultat på grund av metodens enorma känslighet för provets placering i mätinstrumentet. Däremot, om denna känslighet kan tyglas med hjälp av en försöksuppställning som placerar alla prover på exakt samma sätt kan instrumentets höga känslighet göra metoden användbar. Det är därför möjligt att användning av vågledare inom mikrovågsspannet kan bli en användbar metod för att karakterisera kolpartiklar i framtiden.

Nyckelord: black carbon, elementärt kol, partikulärt kol, sot, fullerene C_{60}, impedans, dielektriskt material, snösmältning, kapacitans, vågledare

PREFACE

POPULÄRVETENSKAPLIG SAMMANFATTNING

Vid förbränning av ett kolhaltigt material, så som biomassa, fossila bränslen och biobränslen, frigörs mängder av olika kolpartiklar. Partiklarna är små och sprids lätt med vindar och moln för att sedan falla tillbaka till marken med nederbörden. En sådan typ av kolpartikel är sot.

Sot är svart i färgen vilket innebär att sotpartiklar fångar upp solljus i hög grad. Eftersom energi inte kan förintas så omvandlas den uppfångade energin till värme. Detta fenomen bidrar till den globala uppvärmningen av vår atmosfär i flera avseenden. Sotpartiklar som befinner sig i atmosfären påverkar den globala uppvärmingen direkt genom att fånga upp solljuset och släppa ut värme till atmosfären. Då sotpartiklarna sedan faller till marken kan de hamna på en yta som vanligtvis är ljus, så som snö eller is. Ytan får då en mörkare färg vilket leder till att snön/isen fångar upp mer av solens energi och därav smälter i en snabbare takt än tidigare. Eftersom ytan blir mörkare eller till och med smälter bort, minskas även ytans förmåga att reflektera bort solens strålar från Jorden tillbaka till rymden, och leder återigen till att jorden värms upp. Eftersom det finns väldigt många olika förbränningskällor över hela planeten anses utsläpp av kolpartiklar som ett allvarligt miljöhot.

För att kunna ta sig an det här miljöhotet är det viktigt att kunna karakterisera kolpartiklarna för att därav kunna spåra deras utsläppskällor. De metoder som används idag för att karakterisera kolpartiklar är ofta avancerade och tidskrävande. Det är därför viktigt att forskning inom detta område fortsätter så att bättre och enklare metoder kan tas fram. I den här studien undersöktes ett nytt tillvägagångssätt som innefattade mätningar av kolpartiklarnas elektriska egenskaper. Den egenskap som här undersöktes är permittivitet. Permittivitet är ett mått på hur mycket ett isolerande material polariseras när det utsätts för ett elektriskt fält. Olika material polariseras olika mycket, och därav kan permittivitetsmätningar vara ett sätt att identifiera olika kolpartiklar och skilja dem åt. Permittivitet kan mätas på flera sätt och i den här studien mättes elektriska egenskaper som impedans och resonansfrekvensförflyttning, vilket sedan räknades om till permittivitet. Dessa mätningar utfördes med en impedansanalysator och en vågledare.

För att kunna utvärdera de ovan nämnda mätmetoderna studerades filterprover innehållande olika typer och koncentrationer av pulvriserat elementärt kol, dvs rent kol fritt från andra grundämnen. Koltyperna var fulleren C_{60}, flerväggiga kolnanorör, meso-poröst grafitiskt kol samt sot från en skorsten. Provernas koncentrationer valdes efter vad man tidigare hittat vid snöprovtagning i norra Skandinavien. För att validera dessa koncentrationer utfördes även en fältstudie i norra Sverige där egna snöprover togs och koncentrationsbestämningar gjordes. Koncentrationsbestämningarna påvisade ett kolinnehåll som låg inom det intervall som visats i de tidigare provtagningarna. De kolkoncentrationer som användes till filterproverna ansågs därför stämma väl överens med de som kan hittas i snö i norra Sverige.

Resultaten från impedansanalyserna uppvisade inga tydliga trender mellan permittivitet och mängd kol, vilket troligen berodde på att den mätutrustning som användes inte var anpassad för att med träffsäkerhet kunna mäta på filter av den typ som användes. Därför kunde inte en bedömning göras ifall metoden kan vara av användning vid karakterisering eller inte. Detsamma gällde resultaten från vågledaren som inte kunde bedömas ordentligt eftersom instrumetet hade mycket hög känslighet gällande provets placering i instrumentet. Denna känslighet gjorde att det med tillgänglig utrustning inte var möjligt att med tillräcklig precision placera proverna på exakt samma plats vid alla mätningar. Den här känsligheten i instrumentet visar dock på att den kan uppfatta mycket små skillnader mellan proverna, vilket är en viktig egenskap vid karakterisering av kolpartiklar då det kan vara mycket små skillnader mellan olika typer av kolpartiklar.

WRITING DISTRIBUTION OF REPORT

The following table describes which parts of this report that has been accomplished by either Joakim or Madeleine. All practical moments, such as laboratory work, dielectric measurements and field work has been performed of equal part by Joakim and Madeleine.

	Section in report	Written by
	ABSTRACT	Joakim
	REFERAT	Joakim
	PREFACE	Joakim & Madeleine
	POPULÄRV. SAMMANFATTNING	Madeleine
1	INTRODUCTION	Madeleine
1.2	Objectives	Joakim & Madeleine
1.3	Research questions	Joakim & Madeleine
2	BACKGROUND	
2.1	Terminology	Madeleine
2.2	Dispersion of EC	Joakim
2.3	Background of methods	Madeleine
3	THEORY	
3.1	Dielectrics and permittivity	Joakim
3.2	Capacitance	Joakim
3.3	Impedance	Joakim
3.4	Permittivity extraction with cavity resonator	Madeleine
3.5	Optical depth	Joakim
4	MATERIALS AND METHODS	
4.1	Sample materials	Madeleine
4.2	Preparations of filters	Joakim & Madeleine
4.3	Measurements with spectrophotometer - Aqueous susp.	Joakim
4.4	Measurements with spectrophotometer - On filters	Madeleine
4.5	Measurements with PSAP	Madeleine
4.6	Measurements with impedance analyzer	Joakim
4.7	Theoretical frequency shift calculations	Joakim
4.8	Measurements with cavity resonator	Joakim & Madeleine
4.9	Permittivity calculations from cavity resonator measurements	Joakim
4.10	Snow sampling in northern Sweden	Madeleine
4.11	Estimation of volumetric particle concentrations in meltwater	Joakim
5	RESULTS	
5.1	UV/Vis spectrophotometry - aqueous suspensions	Madeleine
5.2	UV/Vis spectrophotometry - on filters	Madeleine
5.3	PSAP	Madeleine
5.4	Impedance analysis	Madeleine
5.5	Theoretical frequency shifts	Joakim
5.6	Cavity resonator	Joakim
5.7	Permittivity from cavity resonator measurements	Joakim
5.8	Comparison of volumetric particle concentrations in meltwater	Madeleine
6	DISCUSSION	
6.1	Determinating concentrations using spectrophotometry and PSAP	Joakim & Madeleine
6.2	Feasibility of using impedance analyzer measurements as a way of characterizing EC and soot particles	Joakim & Madeleine
6.3	Feasibility of using cavity resonator measurements as a way of characterizing EC and soot particles	Joakim & Madeleine
6.4	Relative permittivity of EC and soot particles as a function of filter mass loading	Joakim & Madeleine
6.5	Limitations	Madeleine
6.6	Recommendations for future studies	Joakim & Madeleine
7	CONCLUSIONS	Joakim & Madeleine

TABLE OF CONTENTS

1 INTRODUCTION

Carbon, the sixth element in the periodic table, has for long fascinated people because of the many different forms it can attain. The carbon atoms can bond into different shapes and create materials as black and brittle as charcoal, as thin and soft as graphene, and as clear and hard as diamond. All these materials consist solely of the element carbon and are therefore commonly said to consist of elemental carbon (EC). Carbon can form a large variety of compounds with other elements and is the basis of all organic matter, and therefore also the basis of life on Earth (Park & Allaby, 2017; Qin & Brosseau, 2011).

Various forms of particulate carbon made primarily or entirely of EC are commonly dispersed in air, precipitation, surface water and soils from both natural and manmade sources. One such type of particulate carbon is soot. Soot is created from incomplete combustion of organic carbon (OC) and can be found e.g. stuck to the inside walls of chimneys (Andrae & Gelencsér, 2006). Depending on what the burned OC consisted of, such as biomass, fossil fuel or biofuel, the soot can have a variety of different properties such as shape, size and composition (Medalia & Rivin, 1982). However, the characteristic dark color is a property that soot as well as other carbonaceous particles have in common (Atkins & Escudier, 2013). Therefore these types of aerosols are often designated under the collective expression "black carbon (BC)", meaning that they strongly absorb light of all wavelengths.

The light absorbing ability of BC aerosols influences the global climate through numerous mechanisms. In a recent report, the U.S. Environmental Protection Agency summarizes the key mechanisms (EPA, 2012). BC absorbs both incoming solar radiation and outgoing radiation, emitted from the surface of the Earth, and re-emits thermal radiation. Therefore, BC particles emitted to the atmosphere contribute to global warming. If the emitted BC particles are deposited on snow or ice they blacken the surface and thereof reduce the albedo. This implies that the snow and ice cover reflect less solar radiation and can therefore melt at a faster speed. Another issue with BC aerosols is their ability to adsorb other pollutants to their surface. BC has a large surface area where pollutants such as polycyclic aromatic hydrocarbons (PAHs) and mercury can be adsorbed. These otherwise volatile pollutants can then get deposited and spread in soils, snow, water and other environments (Elmquist et al., 2007; Wang et al., 2010). The small BC particles can travel over great distances, and it is hard to control emissions since they originate from many kinds of combustion sources. Because of the many affecting factors it can be difficult to characterize the composition and properties of BC particles.

In addition to BC particles emitted by combustion processes, many different types of artificial EC particles can be introduced in the environment by human activities. The industry of carbon nanoparticles, such as carbon nanotubes and fullerenes, is growing with an expanding field of applications, which leads to an increasing risk of dispersion of these particles in the environment (Aitken et al., 2006; Wang et al., 2014). Understanding the behavior of these particles in environments such as water, soils, sediments and biota is important in order to perform environmental risk assessments (Hassellöv et al., 2008).

There are many methods today for quantifying EC and BC in air or water, like SP2, ISSW, OC-EC analysis and thermal-optical analysis. However, many of these methods are time-consuming and do not give adequate knowledge about environmentally-relevant properties such as the specific surface area, degree of crystallinity, and carbon content in particles (Schwartz et al., 2015; Schwarz et al., 2012; Yttri et al., 2014). In this study, alternative methods for characterizing carbonaceous particles were tested. The approach was to expose EC and BC particles to microwaves and measure the dielectric properties of the particles at these frequencies. Carbonaceous particles are good at absorbing microwaves, and therefore this is potentially a good characterization method (Hotta et al., 2011). The permittivity indicates that the particles have electrical properties and is one of the most important parameters of dielectric materials (Kanpan et al., 2012). Because of this, many have been interested in clarifying the relation between the permittivity of EC particles and their characteristics, which has led to an increasing number of publications in this area (Hotta et al., 2011). Detailed information about this relation could help engineers and scientist to improve many research areas, such as capacitors, conductors and medical treatments (Kanpan et al., 2012;

Langa et al., 2012; Dimitrov et al., 2012; Huang et al., 2016). However, dielectric measurements are difficult to perform directly on carbonaceous aerosols since there are no practical means of applying a stable connection to the sample material in air (Cuenca et al., 2014). To bypass this issue, the carbon particles can be collected in precipitation, dispersed in water and filtered. In this way, filters with different carbon particle loadings can be prepared and their dielectric properties measured. The method is also relatively simple and non-destructive, which means that several runs and experiments can be done using the same sample. This is both cost and time efficient as fewer sampling and lab procedures are necessary.

1.1 OBJECTIVES

The aim of this study was to investigate the feasibility and relevance of using dielectric property measurements as a rapid, non-destructive method to characterize and/or discriminate between different types of EC dispersed in the natural environment. This was accomplished through a series of controlled laboratory experiments using various types of EC particles and soot to compare their relative permittivities. In addition, particulate matter deposited in snow was collected from a series of locations in northern Sweden in order to establish the range of BC concentrations and deposition rates expected to be found near pollution point sources such as power plants and settlements. These materials can later be used for further testing of the methods developed in this thesis.

The topic addressed in this thesis is important since developing a fast and non-destructive method for discriminating between various types of carbon particles could, in a relatively simple way, help reveal the pollution sources from which such carbonaceous particles are released. Furthermore, this could, in turn, help to reduce and/or prevent emissions of particulate carbon, but also of other pollutants that could have adhered to the carbon particles, to the environment.

1.2 RESEARCH QUESTIONS

The following research questions were addressed in the study.

A) Can measurements with an impedance analyzer in the microwave frequency range be a valid method for characterizing elemental carbon particles and soot?

B) Can resonant cavity measurements with a rectangular waveguide in the microwave frequency range be a valid method for characterizing elemental carbon particles and soot?

C) How does the relative permittivity of elemental carbon particles and soot, measured in the microwave range, vary as a function of their mass concentration in aqueous suspension and/or mass loading on filters?

D) What concentrations of deposited BC can be found in the meltwater from snow in northern Sweden, and would these concentrations be sufficient to allow the above mentioned methods to be applied for their characterization?

2 BACKGROUND

Measurements at microwave frequencies for studying carbon particles can be divided in two different approaches, resonant and nonresonant methods. Both approaches were used in this study.

2.1 TERMINOLOGY

The terminology of carbon particles can be perplexing since there are a great variety of definitions based on different aspects such as sources, morphological characteristics, chemical composition and optical properties (Andreae et al., 2006). EC, soot and BC are the terms used in this study where EC refers to carbon particles that consists purely (or nearly purely) of carbon atoms. Soot is the sticky black material found in chimneys, created from incomplete combustion of carbon material, and BC is a collective term for carbon particles with high absorption of light. This means that all EC types and soot are included in the term BC, although BC is typically applied to carbon particles in nature, but not to artificial carbon nanoparticles manufactured for industrial processes. These artificial carbon particles are commonly called "engineered carbon-based nanomaterials" (CNMs).

2.2 DISPERSION OF EC

Most EC particles are hydrophobic making them difficult to disperse in water. Fullerenes for example form aggregates when surrounded by water. The particles forming these aggregates are affected by different factors in the environment such as pH and ionic strength (Hassellöv et al., 2008). Like fullerene, CNTs also create complex aggregates due to their low solubility in water. These properties make both fullerenes and CNTs difficult to dose and characterize in aqueous suspensions. There are however methods to enhance the dispersion in water by sonication, adding strong acids (Nowack & Bucheli, 2007), adding surfactants (Jiang et al., 2003) and/or addition of natural organic matter (Hyung et al., 2007).

2.3 BACKGROUND OF METHODS

In previous studies, investigators exposed different kinds of carbon particles to microwaves (300 MHz to 300 GHz) with different experimental set-ups and instruments, and studied the results (Atwater & Wheeler, 2004; Cuenca et al., 2014; Dai et al., 2013; Liu et al., 2010). Generally, two different approaches were used: resonant and nonresonant methods. Resonant methods function at a single, or several discrete, frequencies and give accurate information about the dielectric properties at the specified frequency or frequencies. Nonresonant methods function over a continuous frequency span and give more general information of the electromagnetic properties in this range. To obtain a full picture of the dielectric properties, these two measuring approaches can be used in combination (Chen et al., 2004a).

The cavity perturbation technique, which was used in this study, is a resonant method that has been frequently used since its discovery over 70 years ago (Waldon, 1960; Azzeer et al., 1985; Lobato-Morales et al., 2010). The technique is based on the difference in electromagnetic properties between an empty and partially loaded resonant cavity. A critical difficulty with this technique is to place the samples in the same position during each measurement, which often has an impact on the accuracy of the technique (Estin & Bussey, 1960). This technique has been used to study the permittivity of numerous carbon materials, to approximate if these materials have a suitable permittivity for different applications, often in the electromagnetic area (Miao et al., 2015; Obrzut et al., 2014; Cuenca et al., 2015). Another nonresonant technique that is well used is measurements with an impedance analyzer. By measuring the impedance of a sample, the permittivity can be extracted (Taberna et al., 2002; Liu, 2010).

3 THEORY

In this section important concepts and mathematical and physical expressions used in the study are explained and briefly described. The key concepts explained are impedance, dielectrics, permittivity, capacitance, frequency shift and optical depth.

3.1 DIELECTRICS AND PERMITTIVITY

A dielectric material is defined as a material which is insulating (or have very poor conductivity), meaning that no electrical charges can flow through the material when placed in an electric field at a specific frequency. Instead the material is polarized, which means that the charges inside the material organizes in such a way as to reduce the effect the electric field has on the dielectric material. Different materials are more or less susceptible to the effects of an electric field since some materials are more easily polarized than others (Law & Rennie, 2015a). This degree of polarization is called the permittivity (ε) and is quantifiable. If the frequency of the electric field increases the charges in the dielectric material become more organized. However, at a certain point the frequency change becomes larger than the polarization rate of the material, and an energy loss appears. To be able to describe this phenomenon, the permittivity is written as a complex term, where the imaginary part corresponds to the energy loss (Pozar, 2012b).

$$\varepsilon = \varepsilon' - \varepsilon'' \tag{1}$$

Where ε' is the real part of the permittivity and ε'' is the imaginary part. If the measured energy losses are very small, only the real part of permittivity is taken into consideration:

$$\varepsilon = \varepsilon' \tag{2}$$

The ratio between the permittivity of a material and the permittivity of vacuum (ε_0) is called the relative permittivity (ε_R) or the dielectric constant of the material. However, the permittivity is not constant. Different materials have different permittivities, and the permittivity varies with frequency for the same material. Because of this the relative permittivity can be used to determine material types at chosen frequencies. Equation (3) defines the relative permittivity (Law & Rennie, 2015b):

$$\varepsilon_R = \frac{\varepsilon}{\varepsilon_0} \tag{3}$$

where $\varepsilon_0 = 8.854 \cdot 10^{-12}$ [F/m] (Pozar, 2012a).

3.2 CAPACITANCE

By separating two conductors (here denoted A and B) with an insulating material a capacitor is formed, which has the ability to store electric energy. Connecting the capacitor to e.g. a battery will cause electrons to transfer from one of the conductors (A) to the other (B), giving conductor A a positive charge and conductor B a negative charge of the same magnitude. In other words, there is now a potential difference (V_{AB}) between the two conductors equal to the voltage of the battery. The ratio between the magnitude of the charge (Q) on each conductor and the potential difference between the two is called the capacitance (C).

$$C = \frac{Q}{V_{AB}} \tag{4}$$

A greater capacitance yields a greater charge on each conductor and the ability to store more energy. The capacitance is measured in farad, F = coulomb/volt (Young & Freedman, 2012a). If the insulating material in a capacitor is a dielectric material the capacitance is expressed by:

$$C = \varepsilon \cdot \frac{A}{d} \tag{5}$$

where ε is the permittivity of the dielectric material, A is the cross sectional area of the conductors and d is the thickness of the dielectric material (Young & Freedman, 2016a).

When capacitors are placed in a circuit they can be either placed in series (C_{series}) or in parallel $(C_{parallel})$ with other electrical components. Depending on the positioning of the capacitors the current passing through the circuit behaves differently (Young & Freedman, 2016b).

3.3 IMPEDANCE

Impedance (Z) is a measure of the opposition in a circuit which limits the magnitude of a passing alternating current. When studying a direct current circuit this is called the resistance (R), while in an alternating current circuit an additional factor representing the imaginary part, the reactance (X), has to be taken into account. The relation between impedance, resistance and reactance is the following:

$$Z = R + iX \tag{6}$$

where the resistance is the real part of the impedance and the reactance constitutes the imaginary part. The ratio between the real and imaginary parts of the impedance shows the difference in phase (θ) between the voltage and the current in the circuit (Law & Rennie, 2015c). With a capacitor present in a circuit the difference in phase is negative.

With $C_{parallel}$ and the magnitude of the impedance $(|Z|)$, the relative permittivity for a specific frequency (f), can be calculated with the following formula:

$$\varepsilon_R = \varepsilon_0 \cdot \frac{C_{parallel} \cdot d}{A} \tag{7}$$

where d is the thickness of the dielectric material between the capacitors conductors, A is the area of the conductor in contact with the material and $C_{parallel}$ is:

$$C_{parallel} = -\frac{X}{\omega \cdot |Z|^2} \tag{8}$$

where ω is the angular velocity of the alternating current system. The reactance and the angular velocity can be rewritten to the following:

$$X = |Z| \cdot sin(\theta) \tag{9}$$

$$\omega = 2\pi f \tag{10}$$

where θ is the phase of the impedance. Equation (7) to (10) together gives the following equation for the relative permittivity (Olsson, 2017):

$$\varepsilon_R = \varepsilon_0 \frac{d}{A} \left(\frac{sin(\theta)}{2\pi f |Z|} \right) \tag{11}$$

3.4 PERMITTIVITY EXTRACTION WITH CAVITY RESONATOR

One way to measure permittivity is by using a waveguide resonator connected to a Vector Network Analyzer (VNA). A waveguide can have many different shapes. The waveguide used in this study is a hollow rectangular box with a slit in one side (thoroughly explained in section 4.8). When inserting an object into the slit a shift in resonant frequency occurs. This is visualized on the VNA where the peak at the resonant frequency is displayed.

Following the small perturbation theory, an expected frequency shift can be theoretically calculated using the following formula (Pozar, 2012d):

$$FS = f_0 \frac{(\varepsilon_{eff} - 1) V_{sample}}{2V_{cavity}} \tag{12}$$

where FS is the frequency shift, V_{sample} is the volume of the sample inside the cavity, V_{cavity} is the volume of the cavity, f_0 is the idle resonant frequency and ε_{eff} is the effective relative permittivity of the inserted sample. It is necessary to calculate the effective relative permittivity when the sample constitutes of several different materials. In this study the sample consisted of carbon particles placed on quartz filters, meaning that an relative effective permittivity of carbon and quartz was needed. By using the Maxwell Garnett formula (Equation 13) the effective permittivity can be calculated (Choy, 2016):

$$\varepsilon_{eff} = \varepsilon_m \frac{2\delta_i(\varepsilon_i - \varepsilon_m) + \varepsilon_i + 2\varepsilon_m}{2\varepsilon_m + \varepsilon_i + \delta_i(\varepsilon_m - \varepsilon_i)} \tag{13}$$

where δ is the volume ratio of the two sample materials, ε_i is the relative permittivity of the added material (here carbon) and ε_m is the relative permittivity of the matrix (here quartz).

3.5 OPTICAL DEPTH

Optical depth is a parameter that defines the rate at which incident light is absorbed as it travels through a medium. To estimate the optical depth at a specific wavelength, the following equation can be applied:

$$I = I_0 e^{-\tau} \tag{14}$$

where τ is the optical depth and I_0 and I are the light intensity through a reference filter and a particle loaded filter, respectively. If I_0 and I can be measured, τ can be extracted using the following equation (Nordling & Österman, 2011):

$$\tau = ln\Big(\frac{I_0}{I}\Big) = -ln(T) \tag{15}$$

where T is the transmittance through a medium, i.e. the ratio of how much light energy that goes through the medium with respect to how much light that fell on it in the first place (Law & Rennie, 2015d).

4 MATERIALS AND METHODS

The approach used in this study was to disperse different types of EC powders and soot into aqueous suspensions, filter the suspensions through quartz fiber filters and subsequently measure properties of the filters with carbon materials using electromagnetic and optical methods. The aim of the investigation was to establish if the mass loading and composition of the carbon particles could be related to the permittivity measurements of the particles.

4.1 SAMPLE MATERIALS

The EC particles and soot selected for this study are presented in Table 1. The three EC types were chosen because of their common use in industries, their reasonable price and availability.

Table 1: *Short summary of properties of the EC materials used in this study. The information about the properties of the EC particles were obtained from manufacturers, except for the density and surface area of fullerene C_{60}, which were taken from Iglesias-Groth & Cataldo (2010) and Chen et al. (1999) respectively. N/A=Not available*

	Carbon type	Outer diam. [nm]	Length [nm]	Spec. surface area [m^2/g]	Carbon purity [%]	Manufacturer & product number
Fullerene C$_{60}$	Hollow, spherical carbon nanoparticles	0.7-1	0.7-1 (same as outer diam.)	48	99.9	Sigma-Aldrich 572500
MWCNT	Multi-walled carbon nanotubes	30-50	10000-20000	60	>95	Cheap Tubes 030106
MPC	Sheet-like graphitic carbon nanoparticles	<500 (particle size)	330	70	99.95	Sigma-Aldrich 699624
Soot	Black, sticky powder from chimneys	N/A	N/A	N/A	N/A	N/A

4.1.1 Fullerene C$_{60}$

As the name indicates this carbon molecule consists of 60 carbon atoms, bonded together in the shape of a sphere. The molecule has notable electronic properties and chemical reactivity which makes it useful in many different application areas, such as photovoltaics, superconductors and in medical care in drug delivery systems and contrast agents (Langa et al., 2012; Mojica et al., 2013). Fullerene C$_{60}$ was first discovered in 1985 when Kroto et al. (1985) vaporized graphite by exposing it to lasers. Since then, many different methods for synthesizing fullerene C$_{60}$ have been explored, and today three techniques are used to produce it commercially: pyrolysis of graphene, radio-frequency-plasma and arc discharge-plasma techniques (Mojica et al., 2013).

4.1.2 Multi-walled carbon nanotubes (MWCNTs)

Carbon nanotubes (CNT) are tubes made of a single or multiple atomic layers of graphene. Their length are typical of a few 10s to 100s μm. If the tube consists in a single atomic layer, it is called a single-walled carbon nanotube (SWCNT). If there are several concentric layers, it is called a multi-walled carbon nanotube (MWCNT). CNTs have extraordinary electrical, chemical and mechanical properties and are frequently used in several science and engineering areas such as analytical chemistry, electronics and electrochemistry. The CNTs are particularly useful in electronic devices, batteries, capacitors, etc. (Dimitrov et al., 2012). Their synthesis can be done with numerous methods, but electric arc discharge, laser ablation of carbon and chemical vapor deposition are the most common (Prasek et al., 2011).

4.1.3 Mesoporous graphitic carbon (MPC)

Mesoporous graphitic carbon (MPC) particles have pores with diameters in the span of 2 to 50 nm. This gives the material a large surface area and strong absorbing properties (Walcarius, 2013). Other important properties of MPC are its thermal and chemical stability and electrical conductivity (Liang et al., 2008; Bastakoti et al., 2013). This makes MPC useful in numerous technical applications such as in energy storage, superconductors and capacitors, and in medical care as drug delivery systems (Huang et al., 2016; Liang et al., 2008). MPCs are synthesized by different techniques such as catalytic activation, carbonization of polymer blends and template carbonization (Kyotani, 2000).

4.1.4 Soot

The term soot is here denoted by the definition of Long et al. (2013) as black sticky particles created from incomplete combustion of biomass and fossil fuels. The chemical composition, and therefore the amount of EC, can vary greatly depending on the combusted material (Medalia & Rivin, 1982). Soot has no applications, it is merely an unwanted byproduct (Watson & Valberg, 2001).

4.2 PREPARATION OF FILTERS

To minimize the risk of contamination most of the laboratory procedures were carried out inside a clean room equipped with a filtered air ventilation system and under laminar airflow hoods. Prior to any manipulations, toluene and non-shedding laboratory tissue paper were used to clean and wipe off any particulate or soluble organics that may have been present on lab equipment.

Munktell-Ahlstrom Micro quartz fibre filters (grade MK 360) with a diameter of 50 mm, were used in this study. These filters are commonly used for different types of analytical methods with particulate carbon, such as multi-wavelength light absorption or thermo-optical analysis of evolved CO_2 gas (Karanasioul et al., 2015; Chen et al., 2004b). The first step in the filter preparation process was to remove any unwanted organic carbon material from the filters by sterilizing them in a Sanyo Gallenkamp muffle furnace heated at 800 °C for 38 hours (including the heat up and cool down time). The sterilized filters were then placed in sterile Petri dishes and sealed inside polyethylene bags, to prevent contamination.

In this study, the aim was to test methods that could be applied to the study of carbonaceous aerosols that are deposited from the atmosphere into snow in the northern regions of Sweden (and similar settings). Therefore, it was important, when preparing artificial samples using EC materials, to use concentrations of particulate carbon similar to that found in snow in such environments. In order to create aqueous suspensions with an EC and soot content that resemble these concentrations, data from previous studies conducted in northern Sweden and Finland were used as a guide (Forsström et al. 2013, Meinander et al. 2013, Svensson et al. 2013). The snow samples analyzed in these studies were either taken in remote and rural areas or in proximity of small towns and villages, and the reported EC concentrations in snow varied considerably, from 0 to 810 μg/kg (Table 2). The EC concentrations in proximity of larger northern Sweden towns were not known a priori, but were expected to be several times higher than in remote areas and villages. Since we in our experiemens wanted to mimic EC concentrations found in real settings, it was considered desirable to prepare filters covering a broad range of EC concentrations.

Table 2: *Concentrations of EC found in snow in northern Scandinavia (Forsström et al. 2013, Meinander et al. 2013, Svensson et al. 2013). These concentrations were used as guidelines for the desired concentrations in experiments*

| | | | **[EC] (μg/kg snow)** | | | | |
| | | | **Percentiles** | | | | |
Site	**Type of site**	**Sampling period**	**min**	**P25**	**P50**	**P75**	**max**
Tarfala, SE	alpine, remote	12 - 14 Jul 2008	-	43	43	61	-
	alpine, remote	5 Dec 2008 - 16 Apr 2009	-	4	15	33	-
Pallas, FI	forest, rural	18 Jan - 23 May 2008	-	31	46	89	-
	forest, rural	6 Mar - 5 May 2005	-	51	78	151	-
	forest, rural	3 Mar 2010	7	-	13	-	140
	forest, rural	4 Mar 2010	9	-	15	-	42
	forest, rural	7 May 2010	0	-	25	-	58
Sodankylä, FI	forest, rural	21 Jan 2009 - 14 May 2010	19	40	63	106	213
	forest, rural	29 Oct 2010 - 6 May 2011	19	32	49	75	181
Abisko, SE	village	24 Jan - 24 Apr 2008	-	28	51	91	-
	village	19 Nov - 23 Apr 2009	-	18	32	42	-
Tyresta, FI	town	17 Feb 2010	53	-	180	-	250
	town	21 Mar 2010	370	-	610	-	810

For the chosen EC and soot particles, an initial concentrated aqueous suspension was made by adding 2 mg of EC/soot, weighted with a Mettler Toledo AE160 scale with a precision of $\pm$ 0.0001 g, to 0.1 L of distilled water in a Pyrex beaker. The suspension was exposed to ultrasounds for 4x15 minutes, using a Biologics Inc. Ultrasonic Homogenizer Model 3000 at 50 % power. This was done to break down particle aggregates and obtain a better dispersion. However the hydrophobicity of the EC/soot made the dispersion in water difficult, as the particles tended to float at the water surface or adsorb to the beaker walls.

From the initial aqueous suspension, six different aliquots were transferred into separate beakers and each was diluted with distilled water to a final volume of 0.25 L. The approximate EC/soot concentrations of the aliquots were 25, 50, 100, 250, 500 and 1000 μg/L, obtained by diluting the initial suspension 800, 400, 200, 80, 40 and 20 times respectively. Blank filters were made by filtering solely distilled water with a volume of 0.25 L.

The diluted suspensions were then filtered through the micro quartz filters using a glass funnel and a hand-operated vacuum pump. Any EC/soot particles that stuck to the beaker walls were rinsed out with distilled water from a squeeze bottle. The bottle was weighed before and after rinsing to obtain the used amount of distilled water to estimate the actual concentration of carbon put through the filter. The glassware was thoroughly cleaned between each filtration using the cleaning procedure mentioned earlier. For each EC type and soot the same procedure was applied. After filtration, the filters were put in separate Petri dishes, with their lids slightly opened, and dried in an oven at 60°C.

All filters were photographed in order to keep a visual archive. A greyscale color chart according to the natural color system (NCS) was placed in the photos as a reference and visual legend, see Appendix A. After this, each filter was cut in half, in such a way as to obtain two filter halves with approximately equal particle loadings. One half of each filter was used for experimental measurements, and the other was kept as an archive.

4.3 MEASUREMENTS WITH UV/VIS SPECTROPHOTOMETER - AQUEOUS SUSPENSIONS

Because of the hydrophobicity of EC and soot, the amount present in the suspensions was uncertain. This is why, prior to the actual filtration, an estimate of the EC/soot content in the aqueous suspensions was made by measuring light absorption using a spectrophotometer operating in the ultraviolet to visible (UV/Vis) wavelength range. To do this, 3 mL of aliquots of each diluted EC/soot suspension were pipetted into a quartz cuvette. The same cuvette was used for each suspension in order to avoid differences in absorption between cuvettes. Light absorption for each suspension was measured on a Hach DR 5000 UV/Vis Laboratory Spectrophotometer. The cuvette was thoroughly cleaned between each measurement with distilled water and toluene. The Hach DR 5000 spectrophotometer operates over a wavelength range of 190-1100 nm, and the entire spectrum was used for the analysis.

To estimate the amount of EC that may have passed through the filter during the filtration process, the light absorption in the filtered wastewater was measured with the spectrophotometer, as described above.

4.4 MEASUREMENTS WITH UV/VIS SPECTROPHOTOMETER - ON FILTERS

To help interpret data obtained from the resonant cavity measurements and impedance analyzer, the particle mass loading per unit area (surface density) of carbon particles on the filters was estimated using transmittance measured with Perkin Elmer LAMBDA 950 UV/Vis spectrophotometer operating in the UV-Vis spectrum, 250-1250 nm. The results from this instrument could not be used to determine exact EC/soot concentrations but could give a ranking showing which filters have a higher surface density of particles, based on light transmittance. A lower transmittance indicated a higher particle surface density since transmittance is a measure of the amount of light absorbed by a material. The procedure was the same as the one used with aqueous particles during the preparation of the filters, except that instead of using a cuvette the filters were placed directly inside the instrument. To compare the results obtained with different particle types, the filter transmittance was measured at one specific wavelength instead of the whole UV/Vis-span. According to Hassellöv et al. (2008) 325 nm is the wavelength typically selected for absorbance detection when analyzing fullerene, which is why it was used in this study.

4.5 MEASUREMENTS WITH PSAP

At the Department of Analytical Chemistry and Environmental Science at Stockholm University a particle/soot absorption photometer (PSAP) was used to obtain a more accurate estimate of the surface density of carbon particles on the filters.

The PSAP apparatus consists of two filter holders that clamps a filter in place between two O-rings. Green light with a wavelength of 510 nm is emitted from a light-emitting diode (LED) and led through the upper O-rings to the filter. The intensity of the light that passes through the filter is measured by detectors beneath the lower O-rings (Figure 1). One voltmeter was connected to each output and the measured intensity was displayed as a voltage.
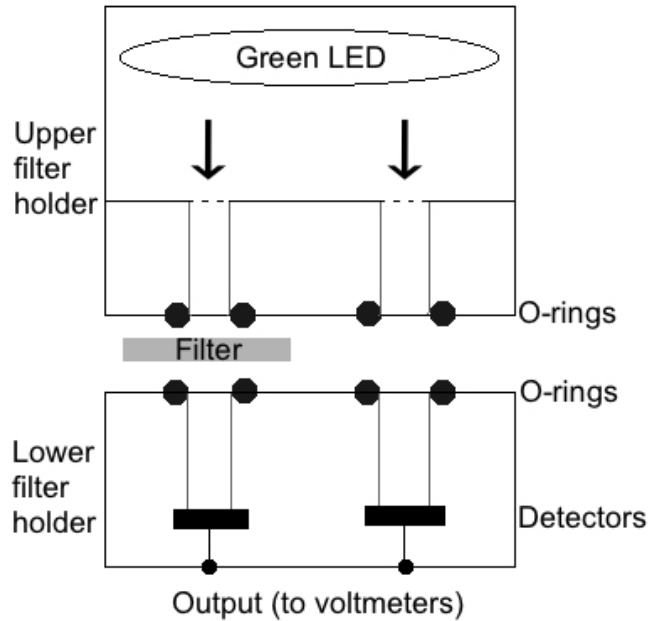
Figure 1: *A schematic cross-section of the PSAP. While measuring, the upper and lower filter holders are clamped, so that no external light reaches the detectors.*

The PSAP is often used for continuous measurements of particles in gases. When measuring continuously a reference filter is needed throughout the whole measurement, which gives an explanation to the two independent identical meters in the PSAP (Bond et al., 1999). In this study, the particles were already on filters so continuous measurements were unnecessary. Instead, both meters were used to obtain two independent results per measurement. One filter at a time was placed under an LED beam, the upper and lower filter holders were clamped together so that the O-rings prevented light from entering or escaping, and the voltage was recorded. The optical depth was then calculated with Equation 15.

4.6   MEASUREMENTS WITH IMPEDANCE ANALYZER

A HP 4291B RF Impedance/Material Analyzer with a Agilent 16453A dielectric material test fixture was used to measure $|Z|$ and θ to evaluate the frequency dependent response of the filtered material with different filter loadings of EC/soot and different types of EC/soot. Measurements were performed in the frequency range of 1 MHz to 1 GHz. Before the measurement session, the impedance analyzer was calibrated using different circuits: open, short, a 50 Ω-load and a PVC sample. On each filter the impedance was measured at three different points, A, B and C to take into account any heterogeneity of the particle distribution (Figure 2).
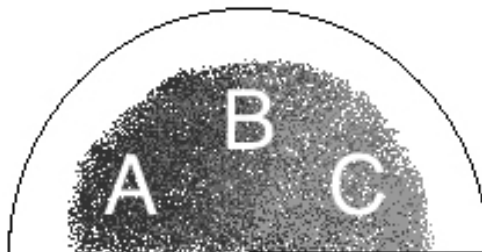
Figure 2: *Schematic figure of a filter with heterogeneous carbon distribution and the three measuring points A, B and C.*

The impedance analyzer measures the amplitude and the phase of the real and imaginary parts of the impedance. ε_R was calculated from the impedance at the frequency 915 MHz, according to Equation 11. This frequency was chosen because it is commonly used in industrial applications (Atwater & Wheeler, 2004). ε_R was plotted against the corresponding concentration of carbon for each EC particle type to investigate any relation. Similarly, ε_R was compared among the different EC particle types at the same specific frequency as mentioned above. For permittivity calculations see Appendix B.

4.7   THEORETICAL FREQUENCY SHIFT CALCULATIONS

Equation 12 was used to calculate the theoretical frequency shift, the frequency shift that should occur with the perturbation method. This was done to put the results from the waveguide measurements in a context. To use Equation 12 an estimate of the effective relative permittivity, of the quartz filter with the EC particles on, was needed. The relative effective permittivity was calculated with the Maxwell Garnett formula (Equation 13). This formula requires relative permittivities for all materials in the sample mixture to be known at the specific resonant frequency examined with the waveguide, which was 12.15 GHz. The relative permittivity of standard manufactured carbon particles at 12 GHz was used for all the carbon standards, which is 7.5 (Hotta et al., 2011). The relative permittivity for quartz is 3.8 on the studied frequency span (Sarafis & Nassiopolou, 2014).

Equation 12 also requires the volume fraction between the carbon and quartz materials. The volume fraction was obtained by calculating the surface densities of EC particles on the filters by using the calibration curve for soot from U.S. National Institute of Standards and Technologies (NIST) (Ström, 2017) and the values for τ achieved from the PSAP measurements (Appendix D). With the density of the particles on the filters and the area of the filter sample inserted into the cavity, the volume of the particles was calculated and compared to that of the entire filter sample. The estimated resonant frequency shift could then be calculated. All calculations were performed in Matlab, see Appendix E for script.

4.8   MEASUREMENTS WTIH CAVITY RESONATOR

A rectangular waveguide was used to measure the complex permittivity of the EC particles loaded on filters. The waveguide was connected to an Agilent Technologies E8364B Vector Network Analyzer (VNA). The waveguide consist of a hollow metal box with a thin slit opening where a sample can be inserted (Figure 4). It is of great importance for the measurements that the samples are of the same volume and placed in the same position inside the cavity (Estin & Bussey, 1960). To minimize any difference between the measurements only a small part of the filters were measured at a time. A hole punch was used to punch out filter pieces with a diameter of 6 mm, two pieces from each filter. One filter piece at a time was placed on a microscope cover glass. The cover glass was marked so that the samples would be put in the same position each time. On top of the sample another cover glass was put, clamping the sample in place between the two cover glasses (Figure 3).

Figure 3: *Cross-sectional view of the sample, clamped between two microscope cover glasses.*

To minimize the positional variation when inserting the sample into the cavity, microscopic glass slides were glued on top of the slit of the waveguide to lock the cover glass in place when inserted (Figure 4). When a sample was inserted into the cavity the frequency shifts of the resonance frequencies could be seen on the VNA's display. The largest frequency shift occurred at the resonant frequency around 12.15 GHz, which is why data were stored only for the frequencies closest to 12.15 GHz. The data were loaded into Matlab and examined in search of a relationship between frequency shift and carbon type and loading.
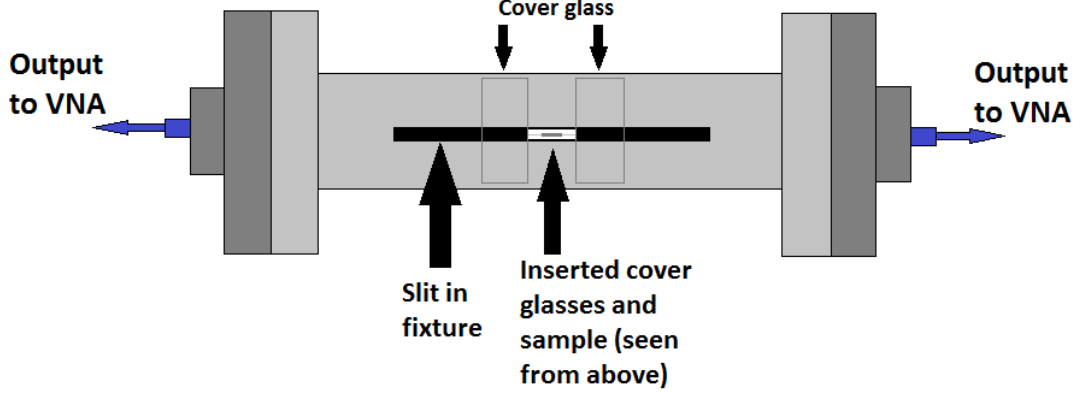
Figure 4: *Schematic picture showing the waveguide with a sample inserted in the slit of the fixture. The sample is a piece of a EC/soot loaded filter clamped between two cover glasses.*

To calculate the frequency shifts, the resonance frequency of the filter with lowest surface density was extracted from the data. The frequency corresponding to approximately the same resonance frequency was then located for the remaining filters. These frequencies were then normalized against the lowest to obtain the shift in frequency between the different surface densities. All calculations were performed in Matlab, see Appendix C for script.

4.9 PERMITTIVITY CALCULATIONS FROM CAVITY RESONATOR MEASUREMENTS

To calculate the relative permittivity of each carbon type, rewritten versions of Equation 12 and 13 were applied. The volume of the microscopic glasses inserted in the cavity and the volume of the quartz filter piece clamped between the glasses were estimated, together named V_{sample}. With the total sample volume, the measured frequency shift and the volume of the cavity, the effective relative permittivity for the combination of glass, quartz and carbon, ε_{eff}, could be calculated with the following formula (rewritten Equation 12):

$$\varepsilon_{eff} = \frac{2 \cdot V_{cavity}}{f_0 \cdot V_{sample}} \cdot FS + 1 \tag{16}$$

With the volume ratio between glass and quartz and with table values for permittivity of both, the effective relative permittivity for the mixture of quartz and glass, $\varepsilon_{g,q}$, were calculated using Equation 13. Further, a rewritten version of the Maxwell Garnett formula was used to calculate the relative permittivity for each EC type respectively:

$$\varepsilon_R = \frac{\delta + 2\varepsilon_{eff} + 2\delta \cdot \varepsilon_{g,q} - 2\varepsilon_{g,q}}{2\delta + 1 + \dfrac{\varepsilon_{eff}}{\varepsilon_{g,q}} \cdot (\delta - 1)} \tag{17}$$

where δ is the volume ratio between carbon and the combination of quartz and glass.

4.10 SNOW SAMPLING IN NORTHERN SWEDEN

A field trip was made in order to collect snow samples to investigate the amount and type of BC aerosols emitted and deposited in snow across northern Sweden during the winter season, when the usage of fossil fuels for commercial, residential or industrial heating is the largest. The time for the trip was chosen to match the highest possible snow accumulation which would also represent the highest accumulation of BC in the snowpack. The maximum snow accumulation is right before the melting period starts, which in northern Sweden is approximately in late March. However, due to unpredictable external events the trip was carried out in early April (2nd to 9th of April 2017). A route was set, with sampling locations downwind from heat power plants and cities as well as in rural and remote areas, see Figure 5. The sampling sites were chosen to provide a representative picture of different possible BC emission/deposition environments.

Nr	Place	Coordinates
1	Umeå	N63°52.138' E20°24.994'
2	Umeå	N63°52.137' E20°25.204'
3	Luleå	N65°37.275' E22°10.252'
4	Gällivare	N67°09.186' E20°43.378'
5	Puoltikas-vaara	N67°26.294' E21°06.075'
6	Kiruna	N67°49.991' E20°15.354'
7	Abisko	N68°21.818' E18°45.571'
8	Jokkmokk	N66°36.340' E19°46.758'
9	Arvidsjaur	N65°32.427' E19°13.342'
10	Lycksele	N64°36.248' E18°43.652'
11	Svartberget	N64°15.354' E19°47.040'
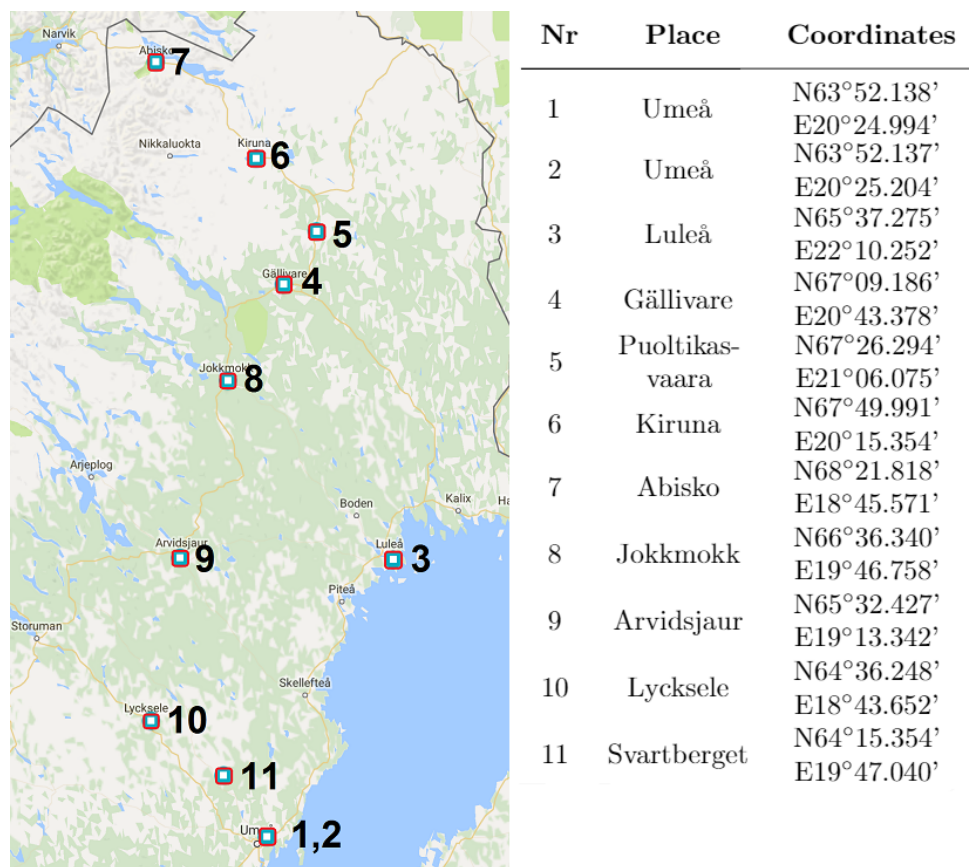
Figure 5: *Map over northeastern Sweden with name and coordinates to the marked sample locations. See Appendix J for complete table over sample locations. Base map produced with Google Maps.*

Wind direction data were collected from Swedish Meteorological and Hydrological Institute (SMHI) (2017) for each site from the 1st to the 14th of April during the last 15 years. Some of the stations were installed more recently than others and had only a few years of data available. Wind roses were created for each site so that the dominant surface downwind direction at each location easily could be determined, there helping to select the most appropriate sampling sites out in the field (Figure 6).
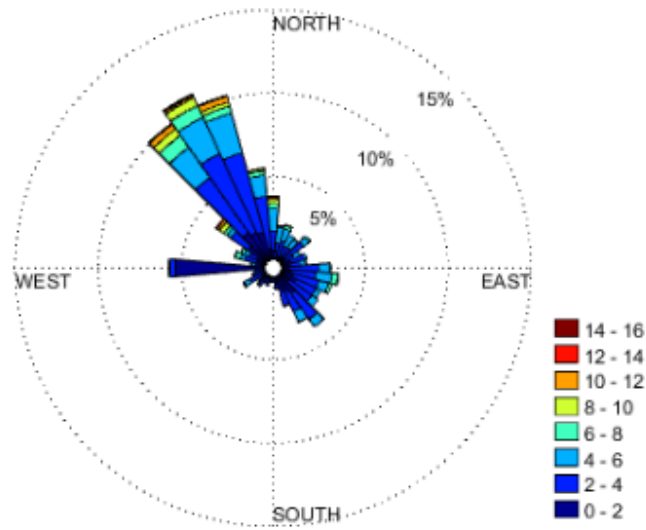
Figure 6: *An example of a wind rose showing the mean predominant wind direction and magnitude in Arvidsjaur during the period 1-14 April (period 2011-2016). In this case, it can be seen that predominant winds are from the northwest. Wind speeds in [m/s].*

4.10.1 Sampling procedure

At each sampling site a pit was dug through the entire seasonal snow layer, with an area of approximately 1 m^2. The environment surrounding the pit was documented both in field notes and photographs in order to record any features that may assist in interpreting findings from the snow sample analyses. The physical structure of the snowpack was examined on one of the snow pit's walls and characterized in terms of snow layer and mean snow grain size. The snow density was measured in the different layers of the snowpack using a 100 or a 250 cm^3 sampler and a spring-loaded scale with a precision of $\pm$ 1 g. The temperature of the snowpack was also measured at different snow depths using a digital temperature probe with a precision of $\pm$ 0.01 °C. Samples representing the entire thickness of the seasonal snowpack were then collected and sealed in plastic bags with a volume of 5 L. Each sample was weighed on a digital scale with a precision of $\pm$ 0.01 kg. The bagged samples were stored inside insulated cooler boxes, made specifically for storage of ice core samples, which maintained them at sub-zero temperatures until they were ready to be processed.

Figure 7: *Upper left: Joakim digging a sampling pit. Upper right: Madeleine taking snow samples from one of the snow pit's walls. Bottom left: Snow pit after sample extraction. Bottom right: Snow samples stored in plastic bags, in line for filtering.*

4.10.2 Sample processing

The snow samples were processed at the research stations at Abisko and Svartberget, which are part of the Swedish Infrastructure for Ecosystem Science (SITES) network. The snow was melted in a microwave oven and then filtered with the procedure as described in section 4.2, with some small modifications. To know how much water that passed through each filter, the beakers used for melting the snow, were weighed both empty and containing the meltwater. The melted snow was pre-filtered through a tea strainer to remove the biggest organic particles, like insects and remnants of plants. Sub-samples of the melted snow were also collected, both before and after filtration. These sub-samples were taken for water chemistry analysis, but these results will not be discussed in this study.

4.11 ESTIMATION OF VOLUMETRIC PARTICLE CONCENTRA-TIONS IN MELTWATER

To compare the volumetric concentrations of the EC/soot particles (used to prepare the filters in the laboratory) with the volumetric concentrations of BC particles in the snow meltwater, PSAP data were first used to obtain particle mass loadings (surface densities) on all filters. Calibration curves were produced through linear regression between the surface densities and the τ-values from the PSAP measurements. Using these calibration curves, estimates of the surface densities of EC/soot in the aqueous suspensions or in the snow samples, could be calculated from their respective measured values for τ. Applying Equation 18, the concentrations of BC (C in Eq. 18) in the meltwater were calculated by inserting the volume of meltwater V used for each snow sample. As the snow samples were expected to contain mainly soot the calibration curve for soot was used to calculate the estimated surface densities for these samples. The volumetric concentration of carbon particles in water (aqueous suspensions or snow meltwater) was then inferred from the following equation:

$$Surface\ density\ = \frac{C \cdot V}{A_{filter}} = \frac{m}{A_{filter}} \tag{18}$$

Where m is the mass of BC and A_{filter} is the filter area covered by particles, which is 9.62 cm^2 for all suspensions.

5 RESULTS

In the following section the results from all performed measurements are presented. The results from the optical methods (spectrophotometry and PSAP) give an insight about the carbon density loadings on the filters, while the electrical methods (impedance and cavity measurements) give an insight of the dielectric characteristics of carbon particle types.

5.1 UV/VIS SPECTROPHOTOMETRY - AQUEOUS SUSPENSIONS

The relationship between absorbance and concentration of the soot suspensions at 325 nm (Figure 8). All suspensions of all standards were analyzed using the spectrophotometer. However, none showed the expected trend of absorbance increasing with increased concentration, which is why only one figure is shown in the report and the others are placed in Appendix F.
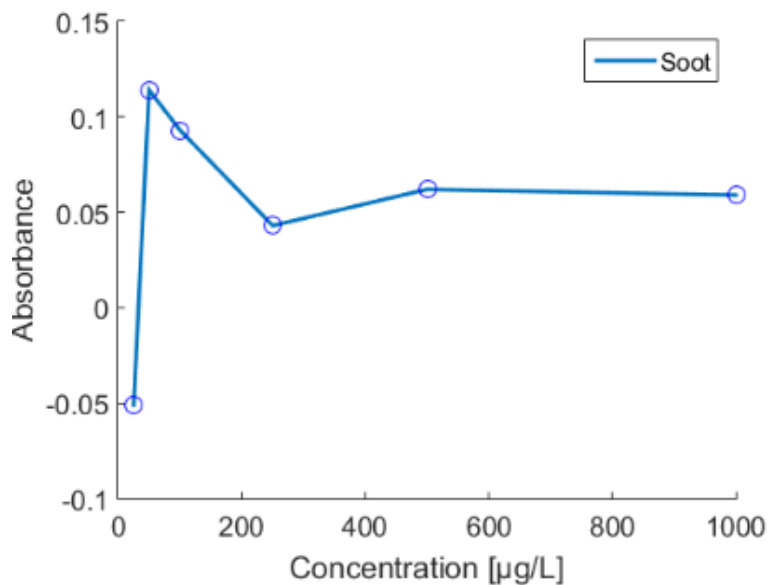
Figure 8: *The absorbance of suspensions containing different amount of soot at the wavelength 325 nm. The circles represent each filter and a line has been drawn between them to better illustrate possible trends.*

Absorbance was also measured in the wastewater from the filtration process. The concentrations appeared too low for the spectrophotometer to detect and negative absorbance values were obtained which is why these graphs were not presented in the report.

5.2 UV/VIS SPECTROPHOTOMETRY - ON FILTERS

The relation between the transmittance and the surface density of the soot filters at 325 nm (Figure 9). An average value calculated from the blank samples is also displayed in the figure for comparison. All standard filters were analyzed, where all except fullerene C_{60} showed the expected trend that transmittance decreases with increasing concentrations. However, the transmittance of the blank filter was still recorded as lower for several filters. The transmittance-concentration relations for the other EC types can be seen in Appendix G.
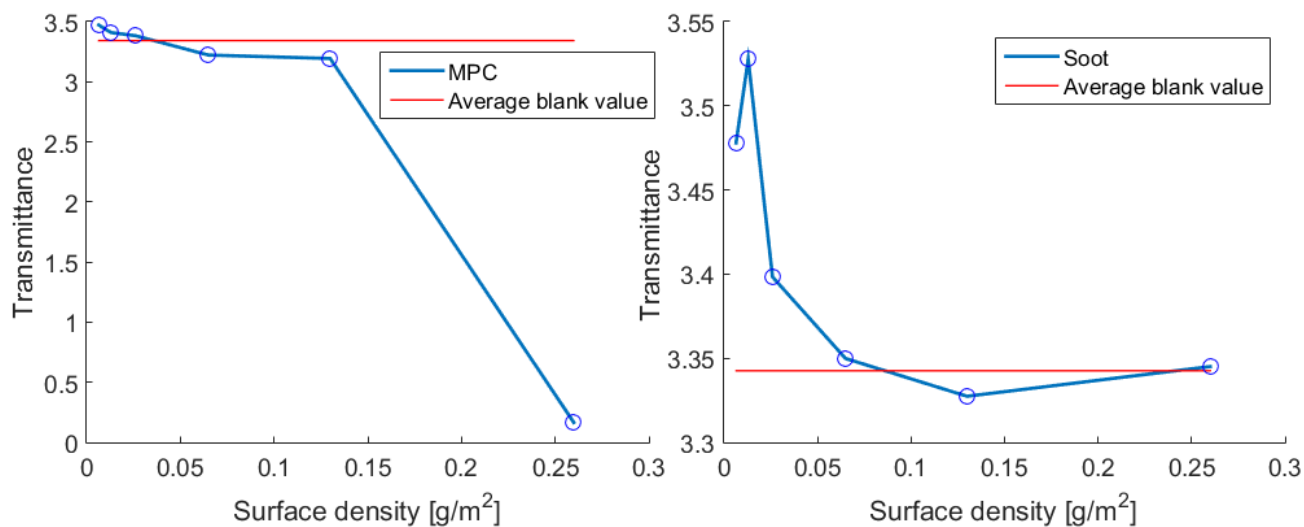
Figure 9: *The transmittance of MPC and soot filters with different estimated surface densities at the wavelength 325 nm. The circles represent each filter and a line has been drawn between them to easier discover possible trends. The average transmittance of the blank filters is shown in red for comparison.*

5.3 PSAP

τ-values for each standard filter were calculated with data from the PSAP measurements and Equation 15. τ increases with increasing surface density, presenting a distinct trend (Figure 10). The slope for each graph in the figure was calculated with linear regression (Appendix H).

Surface densities for all EC and soot filters were estimated using the calculated τ-values and the calibration curve for NIST-soot (Appendix D).

Table 3: *Surface densities of the EC types and soot in [g/m^2] from highest to lowest estimated carbon loading, with filter 1 having the highest estimated loading and 6 the lowest estimated loading.*

Filter	1	2	3	4	5	6
MPC	0.0364	0.0182	0.0079	0.0028	0.0011	3.54E-04
MWCNT	0.0486	0.0212	0.0176	0.0038	0.0028	0.0030
Fullerene C$_{60}$	0.0141	0.0099	0.0035	0.0025	0.0016	0
Soot	0.0300	0.0143	0.0090	0.0038	3.392E-04	0.0026
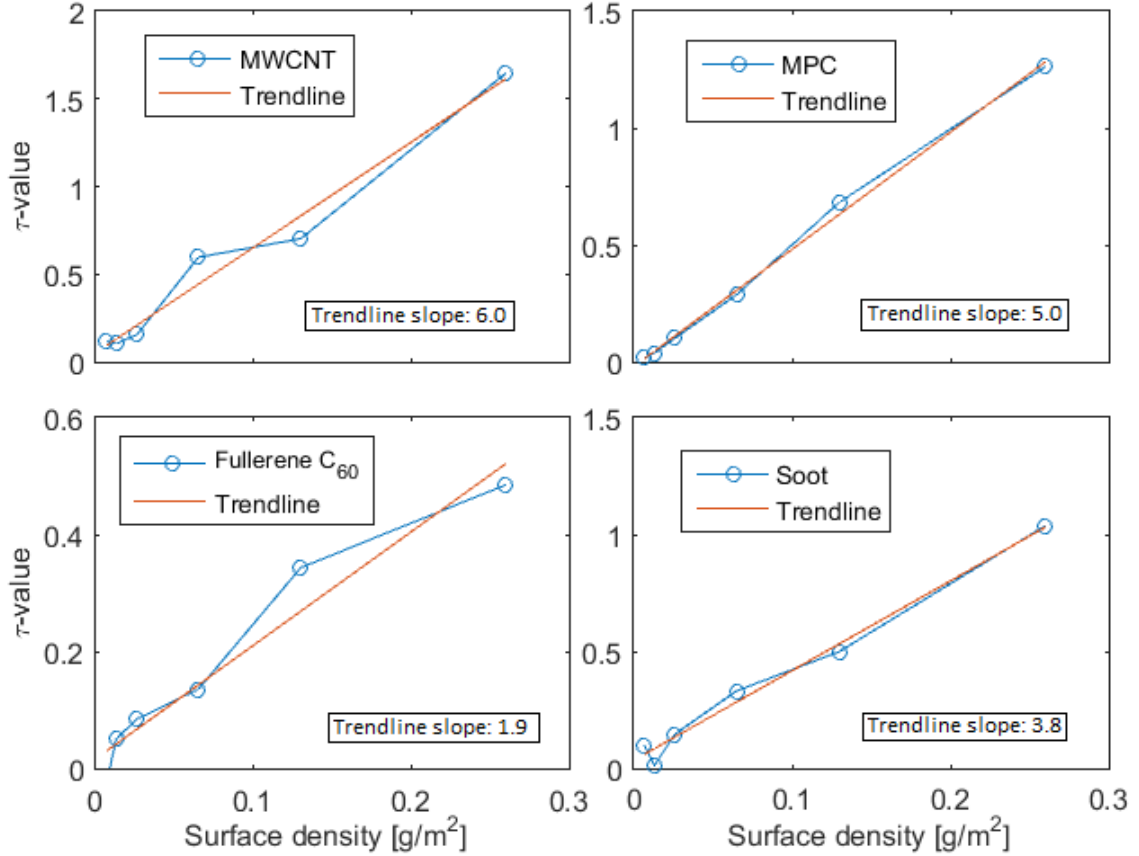
Figure 10: *τ-values for the different standards in relation to the estimated surface density for each particle type. Each circle represents a filter.*

5.4 IMPEDANCE ANALYSIS

To illustrate the variation in relative permittivity (ε_R) between the different filter loadings for each standard types the value of ε_R was calculated at 915 MHz (Figure 11). None of the graphs show any expected trend and the values are well below the relative permittivity of vacuum. The graphs also show that the relative permittivity of the carbon loaded filters are lower than that of the blank samples except for the two MPC filters with the lowest surface density.
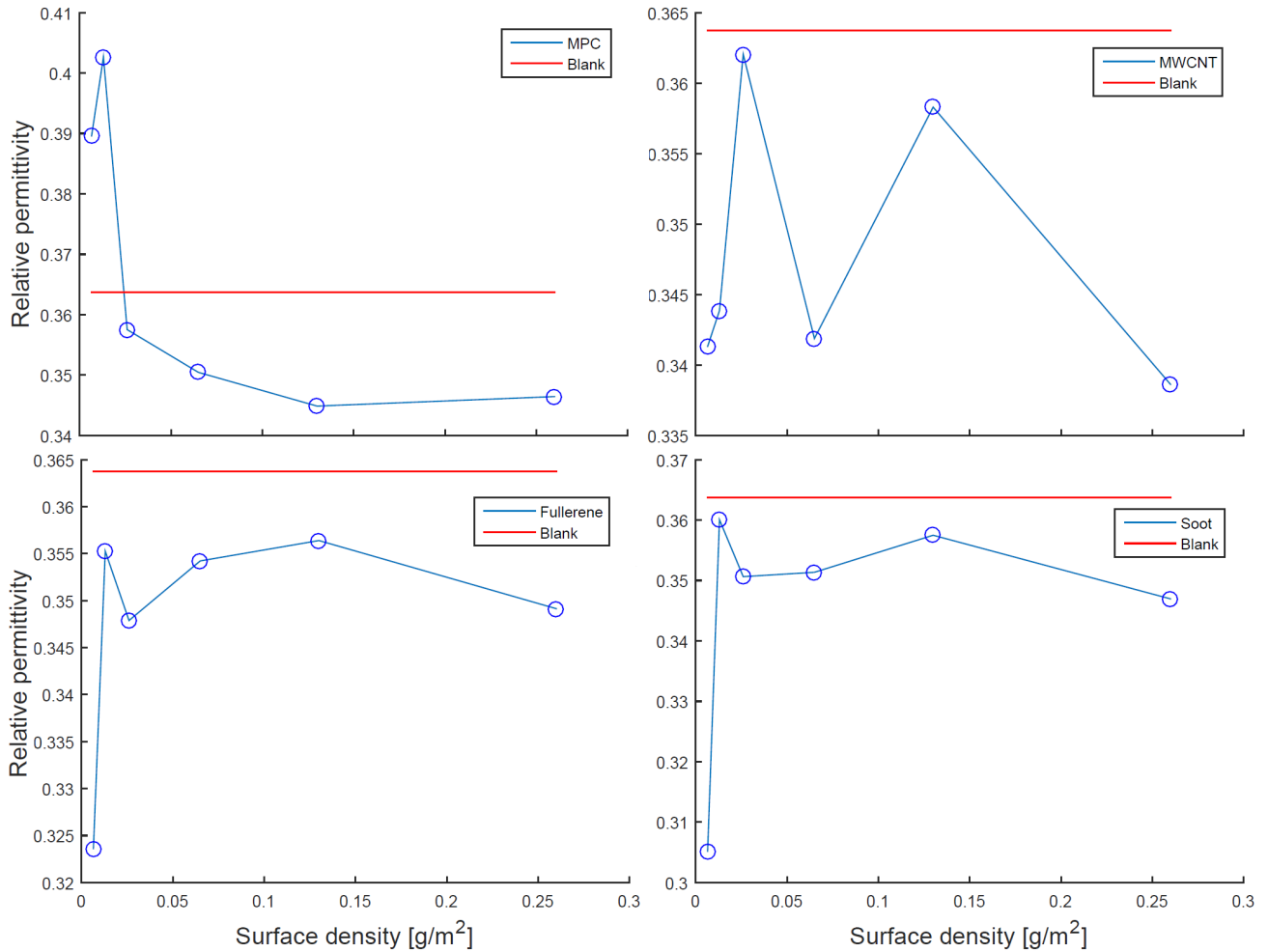
Figure 11: *The relative permittivity at different surface densities for all standard filters in comparison to the relative permittivity of the blank filters (averaged). The circles represent each filter where an average of three measurements was calculated.*

5.5 THEORETICAL FREQUENCY SHIFTS

The effective relative permittivity (y-axis) was calculated using the surface densities (x-axis), which explains the linearity in Figure 12. With the surface densities used in this study the theoretical effective permittivities, calculated using the Maxwell Garnet formula (Appendix E), are in the span 3.8 - 3.801 (Figure 12).
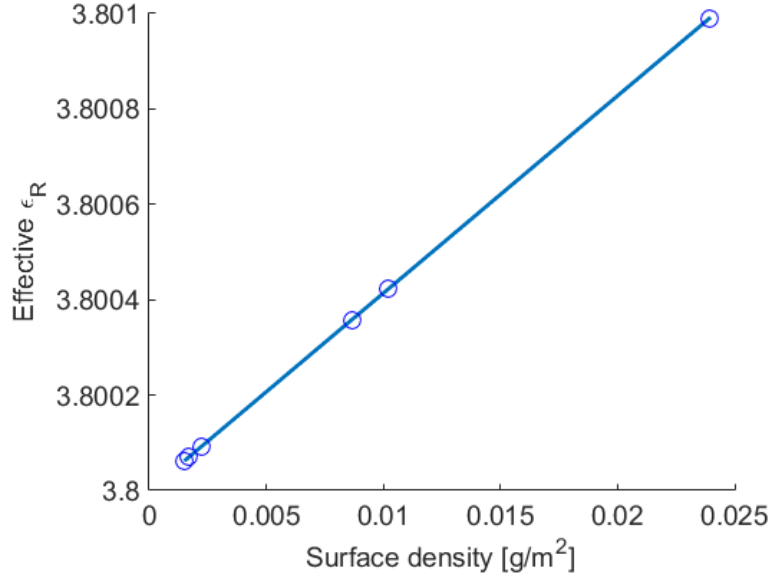
Figure 12: *The effective ε_R values for theoretical filters containing BC (circles), calculated using the Maxwell Garnett formula using the relative permittivities of BC and quartz at 12.15 GHz. The surface densities are calculated using τ-values for the soot particles and were approximated using the calibration curve for NIST soot (Appendix D).*

The differences in theoretical effective relative permittivity are small but the frequency shifts are still distinguishable (in the kHz region)(Figure 13). However, the theoretical frequency shifts are small in comparison to the studied frequency (12.15 GHz).
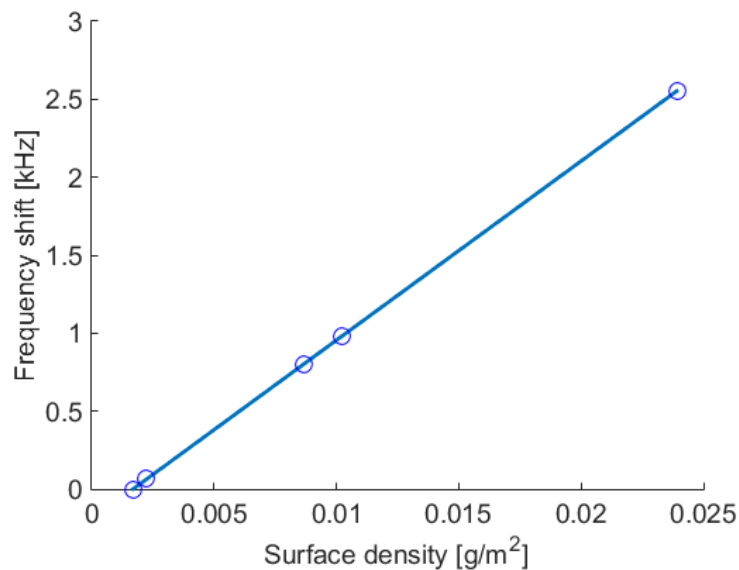
Figure 13: *The theoretical frequency shift as a function of the different surface densities. Each circle represents a theoretical filter.*

5.6 CAVITY RESONATOR

The calculated frequency shifts for each standard is illustrated in Figure 14 in relation to the surface density of the filters. The frequency shifts have been normalized against the filter represented by the lowest frequency of each type, to get a better view over the magnitudes of the frequency shifts. No trends were observed for either standard type.
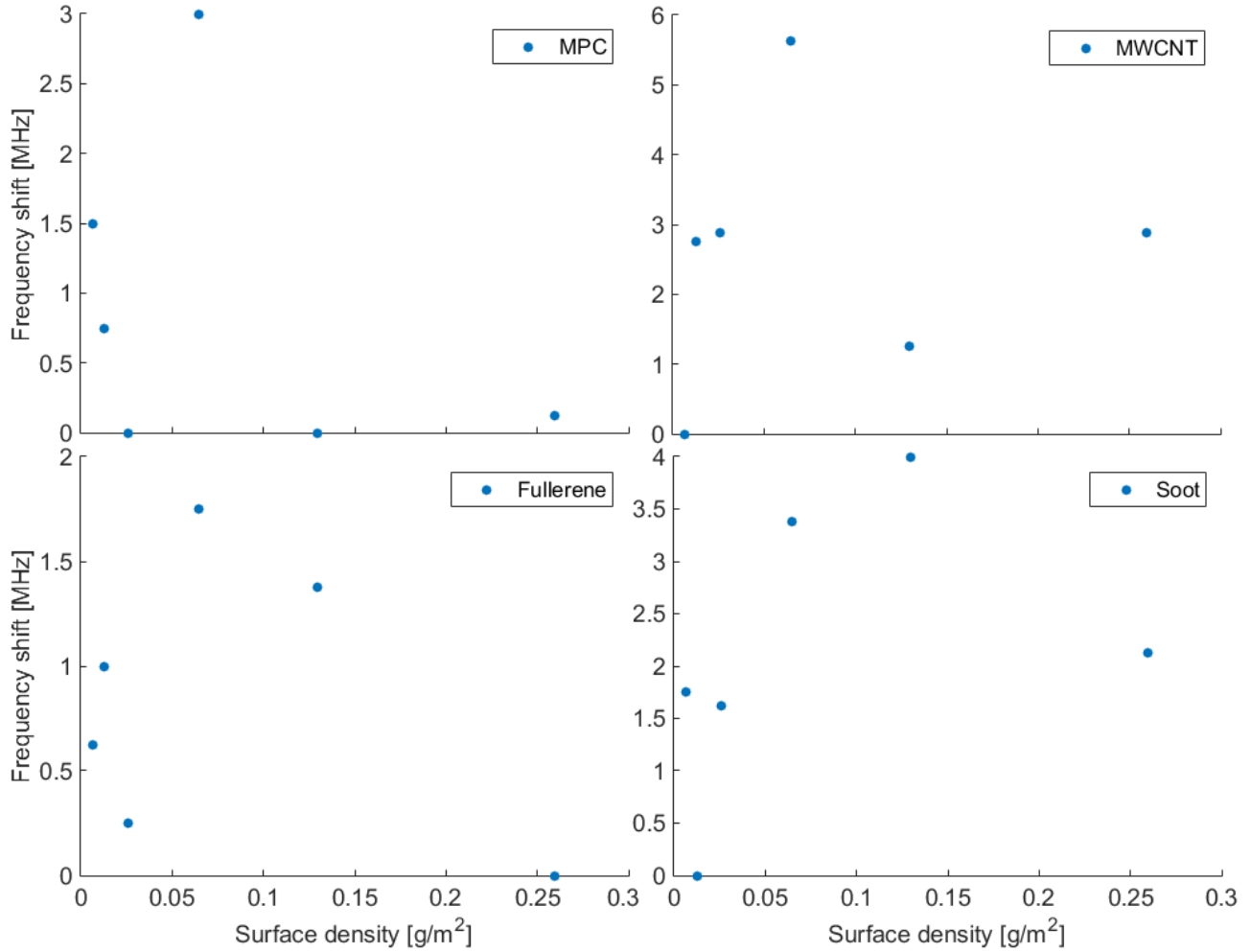
Figure 14: *The frequency shifts for each standard type against surface densities. Each dot represents a filter sample.*

5.7 PERMITTIVITY FROM CAVITY RESONATOR MEASUREMENTS

The calculated permittivies are similar for all EC types. The permittivities decrease slightly with increasing carbon loading. Soot has a slightly lower relative permittivity than the other three EC types (Table 4).

Table 4: *The relative permittivity for each of the EC types examined in this study, calculated using cavity resonator measurements at 12.15 GHz. Filter 1 corresponds to the highest estimated loading and filter 6 to the lowest estimated loading.*

Filter	1	2	3	4	5	6
MPC	12.9080	12.9081	12.9082	12.9083	12.9083	12.9083
MWCNT	12.9076	12.9080	12.9082	12.9083	12.9083	12.9083
Fullerene C_{60}	12.9071	12.9078	12.9079	12.9082	12.9082	12.9082
Soot	12.8908	12.8995	12.9039	12.9066	12.9074	12.9079

5.8 COMPARISON OF VOLUMETRIC PARTICLE CONCENTRATIONS IN MELTWATER

A comparison between the estimated volumetric concentrations of carbon particles in the aqueous suspensions of soot prepared in the laboratory, and BC in the melted snow samples from northern Sweden (Figure 15). Several replicate filters were processed with the meltwater from the same snow sampling site, which is why the same site may have several different BC concentrations.
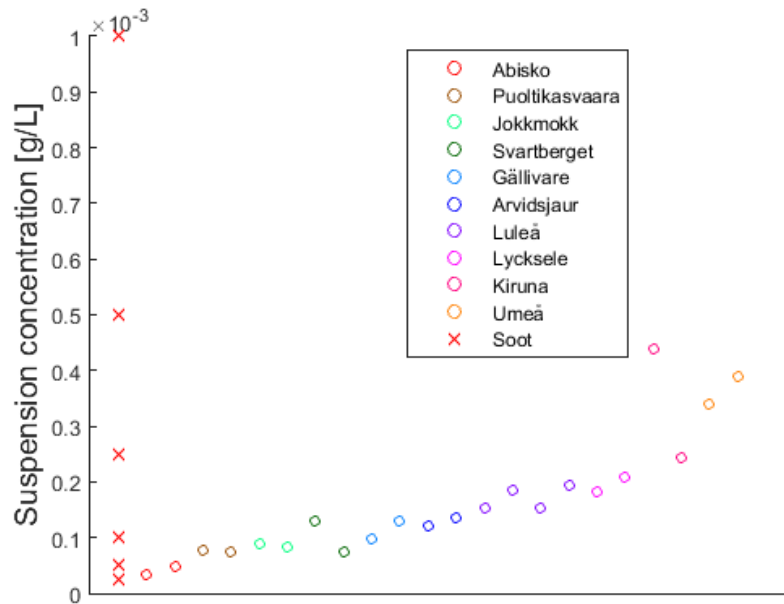
Figure 15: *A comparison between the concentration of BC particles in the meltwater of snow samples and the standard soot samples.*

The BC concentrations in the snow meltwater were between 25 - 500 μg/L. The range of BC concentrations in snow meltwater overlaps well with the range of soot concentrations in the aqueous suspensions prepared in the laboratory. The same pattern is seen for the other EC types (Appendix I). The BC concentrations calculated with the calibration slope for fullerene C_{60} (Appendix H) have a larger span, approximately 50 - 900 μg/L, however this span does not exceed the highest value of the standard fullerene C_{60} concentration.

6 DISCUSSION

The majority of the results indicate that the methods regarding characterization of carbon particles need adjustment to provide good distinguishability between the EC particles. However, there are many different factors that could affect the outcome. These will be discussed in the following sections.

6.1 DETERMINING CONCENTRATIONS USING SPECTROPHOTOMETRY & PSAP

When preparing the suspensions the most diluted aliquot should contain the least amount of carbon particles. Since the particles are known to absorb light, the lowest absorbance from spectrophotometer measurements should be found in the most diluted suspension. However, this is not the case when studying Figure 8 where no obvious trend can be seen. This could be caused by the detection rate of the spectrophotometer being too low to detect the concentrations, but since some of the suspensions have a visible grey color this should not be the case for every suspension. As mentioned in section 4.2 the dispersion of EC and soot is limited by the hydrophobicity of the particles. When preparing the suspensions, particles adhering to the beaker walls could be seen. There was also a small time gap between the preparation of the suspensions and the spectrophotometer measurements, meaning that particles had time to sediment and/or surface. In summary, there are several steps between the preparation process and the measurements that could have an impact on the results.

In contrast to the spectrophotometer measurements of suspensions the spectrophotometric measurements performed on filters show a trend where the transmittance decreases with increasing surface density. This trend was expected since a high surface density originates from a thick layer of particles that limits the amount of light passing through the filter, and therefore results in a lower transmittance. However, for all standard types the spectrophotometer detects a transmittance higher than that of the average blank for at least one filter. There is no simple explanation to this as there are several different factors to consider. The detection limit of the spectrophotometer could be too low to detect the loadings. It could also be that the filters in prior measurements had been contaminated, worn or that some particles were detached from the loaded filters during measurements.

The PSAP measurements were performed multiple times using two independent detectors to minimize variations in the result. Both of the detectors showed similar values for the optical depth of each filter. These values indicated a trend where surface densities correlate to the concentrations used to prepare the filters. This shows that the surface densities follow the expected order of magnitude despite uncertainties in concentrations due to the difficulties when dispersing the particles. This implies that measurements with a PSAP is a promising method when evaluating EC concentrations on filters. A possibility as to why the PSAP showed better results than the spectrophotometer measurements is that when adding the carbon particles to the filters the beakers were rinsed to ensure that as many of the particles as possible ended up on the filters. Only a small piece of each filter was studied in the PSAP, chosen to represent the entire filter. Some filters could visually be identified as more heterogeneous than others, indicating that a small piece of the filter is less representative. To get a more accurate representation, several sample pieces should have been examined and more measurements should have been performed.

To increase the dispersion rate of the carbon particles in aqueous suspension the addition of a surfactant could prove useful. The concentrations of the prepared suspensions would become more accurate and less time would be spent on concentration measurements. An increased dispersion could also give a more homogeneous distribution of particles, making fractions of a filter more representative for the entire filter. Another option would be to skip the filters and measure the impedance directly in the suspensions, as Aldosky & Shamdeen (2011). This would remove the uncertainty regarding uneven particle distribution on filters completely. Combining this method with the use of surfactants to prevent the particles from sedimenting, surfacing or adhering to the container would be preferable. The EC and soot particles could also be molded together with a material with known dielectric properties, such as silicon, as in the method by Liu et al. (2010).

This would give us the option to create solid samples of desirable shape and size within the limits of the test fixture. Using solid samples would be preferable as the fraction of air present in the sample would become smaller and the particles could connect directly to one another. However, applying these techniques would cause the samples to deviate much more from the natural occurring state of these particles. The purpose of this study was to examine these particles as if collected in nature which is why these methods were not implemented.

The EC concentrations of the aliquots were chosen to represent concentrations found in snow in northern Sweden (Table 2). When comparing the concentrations in the melted snow samples with the concentrations of the laboratory aliquots, they were all within the same range. This indicates that the chosen EC concentrations are representative for northern Sweden snow. It is however possible that higher filter loadings would have been more suitable for characterization with the methods applied in this study. Using higher loadings in a larger range could unveil more distinct differences in the results between samples.

6.2 FEASIBILITY OF USING IMPEDANCE ANALYZER MEASURE-MENTS AS A WAY OF CHARACTERIZING EC AND SOOT PARTICLES

The results from the impedance measurements all indicate relative permittivities lower than that of vacuum (relative permittivity lower than 1), which is unrealistic. None of the relative permittivities, calculated using data from the impedance measurements, were close to the calculated theoretical relative permittivities. The measured values are at least a factor 10 smaller, even for the blanks. There are several reasons that could explain why the relative permittivites were lower than 1. One significant source of error could be the sample thickness limitation of the test fixture which is designed to measure samples with a thickness between 0.3 - 3 mm. The measured quartz filters were approximately 0.25 mm thick and during analysis the filters were clamped between the electrodes with a high pressure, meaning that the thickness was less than 0.25 mm due to the soft structure of the filters. This might indicate that the instrument did not provide information based on our thin samples but instead worked under the assumption that the samples were much thicker. Equation 11 illustrates the impact of sample thickness on measured relative permittivity, showing a linear correlation between the two. An option would be to use a different fixture designed to measure thin samples. Prior to the measurements the analyzer had to be calibrated. To verify the accuracy of the calibration a test sample of teflon was inserted and the relative permittivity calculated. Regardless of caution when calibrating, the relative permittivity of the teflon was off with approximately a factor 1.5 from the theoretical value. This indicates that a decent calibration was not obtained, which could have affected the results.

A similar setup, as the impedance analyzer and fixture, was used by Liu et al. (2010) where samples of MWCNTs, silicon and a hardener were molded. The molding procedure gave the authors the option to create thicker samples appropriate for the fixture (the same type of Agilent fixture as in this study). They used a minimum of 1 wt% in their samples, meaning that they had an amount of MWCNTs at least 10 times larger per sample than in this study. With this amount of MWCNTs they found a relative permittivity for the mixture of 9, but when using greater amounts of carbon (50 times more than our highest loading) they achieved even higher relative permittivities. These high values could be caused by the addition of the hardener, whose permittivity however is not mentioned in their report.

In summary, the method with the impedance analyzer as applied in this study is not a reliable method for characterizing EC or soot. However, we can not righteously reject the method. Liu et al. (2010) used a similar method and acquired good results, which shows that this method has some potential. With a fixture better suited for the thin quartz filters, improved calibrations and higher EC loadings on the filters, the use of the impedance analyzer is potentially to be an appropriate method to characterize EC or soot.

6.3 FEASIBILITY OF USING CAVITY RESONATOR MEASUREMENTS AS A WAY OF CHARACTERIZING EC AND SOOT PARTICLES

The frequency shift of the different filters inserted into the waveguide are in the MHz region. The theoretical frequency shifts are in the kHz region, indicating that the measured frequency shifts are much greater than what would be expected. As mentioned by Estin & Bussey (1960) this is likely due to the extreme sensitivity of the instrument where the slightest displacement of the sample has a major impact. The impact sample displacement has on frequency shift is larger than the effect of different loadings. However, if this sensitivity could be mastered this technique is likely to give accurate measurements distinguishing both carbon loadings and different carbon types. For example, an external device fixed to the waveguide, limiting the movement of the sample to one dimension (in and out of the cavity), could make this method plausible for characterizing EC and soot.

The relative permittivites calculated from the cavity resonator measurements (Table 4) are for all EC types and loadings very close to 12.9. Hotta et al. (2011) made a study similar to this, where a sample was placed in a sealed waveguide, to calculate permittivities of different carbon compounds and obtained results similar to those in this study. However, it is difficult to accurately interpret the results from Hotta et al. as they had to be extracted visually from a graph. With these approximations a rough comparison was made indicating that the permittivity calculations performed in this study are reasonable.

The studied frequencies are only a small part of the entire range of microwaves. It would therefore be of interest to study the behavior of the EC and soot particles exposed to other microwave frequencies. It is possible that small particle loadings could become more visible at higher frequencies.

6.4 RELATIVE PERMITTIVITY OF EC AND SOOT PARTICLES AS A FUNCTION OF FILTER MASS LOADING

The theoretical effective relative permittivities, for a mixture of EC and quartz, were calculated to 3.800 - 3.801 (higher values with higher carbon loadings) which is very close to the relative permittivity of quartz (3.8). This indicates that the addition of carbon to the quartz filters has a small impact on the effective relative permittivity. This is reasonable since the carbon particles constitutes a very small fraction of the whole sample, while the rest is quartz filter.

The relative permittivities calculated from the cavity perturbation measurements showed a slight increase with decreasing carbon loading for each EC type. These results are opposite to those of the theoretical effective relative permittivites, which revealed higher permittivity with higher carbon loading. However, the increase in the calculated permittivites is small (third or forth decimal) which questions the certainty of the result.

Because of the inconclusive results it is not possible to answer how the relative permittivity of EC and soot varies as a function of their mass concentrations, but a slight variation between the samples is still visible in the results. To reveal the true behavior of this variation further measurements are needed.

6.5   LIMITATIONS

Since this study is a 30 hp master thesis mainly consisting of laboratory analyses, numerous things had to be limited. Everything from quantity of measurements and samples to available instrumentation and equipment had to be considered and often limited due to time and budget. Here follows some limitations worth mentioning:

The method had to involve simple and cheap techniques that are easily replicable by others.

The search for an appropriate method involved measurements on filters loaded with different amounts of carbon. With the prescribed time limit the amount of studied concentrations was limited to six.

The hydrophobic nature of EC and soot made it difficult to disperse in water. However, having a large surface area makes the particles susceptive to other substances that through adsorption functionalize the carbon particles and alters their ability to disperse or dissolve in water. There are multiple ways of manually enhancing the dispersibility of carbon particles in water, like functionalizing them with chemicals or using surfactants. The behavior of the particles in the natural environment is however difficult to predict due to the uncertainty regarding their hydrophobicity. In this study the treatment of the EC is limited to ultrasonication that shatters potential aggregates.

6.6   RECOMMENDATIONS FOR FUTURE STUDIES

This is a summary of recommendations thought of during this study (several are already mentioned in the discussion above):

- Solid samples to minimize thickness variations, air presence and enhance customizability regarding size and shape

- Studying EC at higher frequencies could improve detection of small particle loadings

- Addition of a surfactant to enhance dispersibility of particles and create filters with more accurate and homogenous loadings

- A different test fixture for the impedance analyzer suited for thinner samples

- A different waveguide better suited for the samples or an external device to fixate the sample and limit the displacement

- Additional measurements to determine variational behavior of permittivity between loadings

- Analyze a greater span of carbon loadings (especially higher carbon loadings) to possibly make detection with used equipment easier

7 CONCLUSIONS

Evaluation of the approach for measurements in this study gave us insight in how the methods, through tweaks, could become successful and give accurate information regarding the dielectric properties of EC. Being able to characterize carbon particles, with the purpose of identifying their way of transportation in the environment, is currently a hot topic. Therefore, it is of utmost importance that research in this field of study continues so that a successful method or implementation can be obtained.

Characterizing elemental carbon particles with an impedance analyzer, as applied in this study, was not an adequate method. Through tweaks, such as switching the analyzer for another better suited for the thin soft quartz filter we used, this method should become viable as it is easy to implement.

The experiments with the resonant cavity showed promising results and with the addition of a sample holder this could be valid method for characterizing EC particles and soot.

By measuring with an impedance analyzer unsuited for thin quartz filters and with minor positional differences of the samples inserted into the resonant cavity, no obvious relation between mass concentration and relative permittivity of EC particles and soot was identified. However, there was a slight variation between the samples which indicated that further measurements are necessary to reveal this relationship.

The good correlation between the surface density and the concentrations of the aliquots used to prepare the filters, indicated that PSAP was a suitable method to measure the carbon loading on the filters.

The measured concentrations of BC found in snow sampled in this project were proven accurate as prior concentration measurements, done by others, of northern Scandinavia snow showed similar concentrations. These concentrations were between 25 - 900 μg/L and indicated that highly sensitive instrumentation is required to analyze snow samples as these amounts of carbon particles were fairly low in comparison to those analyzed by others using impedance and cavity resonator analysis.

8   REFERENCES

Aitken, R., Chaudhry, M., Boxall, A., Hull, M. (2006). Manufacture and use of nanomaterials: current status in the UK and global trends. *Occupational Medicine-Oxford*, **56**: 300-306.

Aldosky, H. Y. Y., Shamdeen, S, M. H. (2011). A new system for measuring electrical conductivity of water as a function of admittance. *Journal of Electrical Bioimpedance*, **2**: 86-92.

Andrae, M. O., Gelencsér, A. (2006). Black or brown carbon? The nature of light-absorbing carbonaceous aerosols. *Atmospheric Chemistry and Physics*, **6**: 3131-3148.

Atkins, T., Escudier, M. (2013). Soot (black carbon). In: *A Dictionary of Mechanical Engineering*, Oxford University Press. Available: `http://www.oxfordreference.com/view/10.1093/acref/9780199587438.001.0001/acref-9780199587438-e-5880` [2017-06-09]

Atwater, J. E., Wheeler, JR. R. R. (2004). Temperature dependent complex permittivities of graphitized carbon blacks at microwave frequencies between 0.2 and 25 GHz. *Journal of Materials Science*, **39**: 151-157.

Azzeer, A. M., Silber, L. M., Spain, I. L., Patton, C. E., Goldberg, A. (1985). Applicability of the microwave cavity perturbation method for conductivity measurements on carbon fibers. *Journal of Applied Physics*, **57**: 2529 – 2531.

Bastakoti, B. P., Oveisi, H., Hu, C. C., Wu, K. C. W., Suzuki, N., Takai, K., Kamachi, Y., Imura, M., Yamauchi, Y. (2013). Mesoporous carbon incorporated with In2O3 nanoparticles as high-performance supercapacitors. *European Journal of Inorganic Chemistry*, **2013**: 1109-1112.

Bond, T. C., Anderson, T. L., Campbell, D. (1999). Calibration and intercomparison of filter-based measurements of visible light absorption by aerosols. *Aerosol Science and Technology*, **30**: 582 - 600.

Cheap Tubes. *Multi Walled Carbon Nanotubes 30-50 nm.*
Available: `https://www.cheaptubes.com/product/multi-walled-carbon-nanotubes-30-50nm/` [2017-05-28]

Chen, L. F., Ong, C. K., Neo, C. P., Varadan V. V., Varadan, V. K. (2004a). *Microwave Electronics.* Chichester, West Sussex: Wiley Sons, Ltd. Available: Uppsala University E-Library [2017-05-26]

Chen, A. L. W., Chow, J. C., Watson, J. G., Moosmuller, H., Arnott, P. W. (2004b). Modeling reflectance and transmittance of quartz-fiber filter samples containing elemental carbon particles: Implications for thermal/optical analysis. *Aerosol Science*, **35**: 765 - 780.

Chen, J., Sheng, G., Liu, S., Liu, Z.-Y., Liu, Z.-Q., Fu, J. (1999). BET surface area and porous structure of fullerenes and fullerene soots. *Chemical Research in Chinese Universities*, **15**: 90-93.

Choy, T. C. (2016). *Effective medium theory: principles and applications.* 2nd ed. Oxford: Oxford University Press. Available: Uppsala University E-Library [2017-06-03]

Cuenca, J. A., Thomas, E., Mandal, S., Williams, O., Porch, A. (2015). Investigating the broadband microwave absorption of nanodiamond impurities. *IEEE Transactions on Microwave Theory and Techniques*, **63**: 4110-4118.

Cuenca, J. A., Thomas, E., Mandal, S., Williams, O., Porch, A. (2014).Microwave determination of sp2 carbon fraction in nanodiamond powders. *Carbon*, **81**: 174-178.

Dai, B., Ren, Y., Wang, G., Ma, Y., Zhu, P., Li, S. (2013). Microstructure and dielectric properties of biocarbon nanofiber composites. *Nanoscale Research Letters*, **8**: 293.

Dimitrov, A., Tomova, A., Grozdanov, A., Popovski, O., Paunović, P. (2012). Electrochemical production, characterization, and application of MWCNTs. *Journal of Solid State Electrochemistry*, **17**: 399-407.

Elmquist, M., Zencak, Z., Gustafsson, O. (2007). A 700 year sediment record of black carbon and polycyclic aromatic hydrocarbons near the EMEP air monitoring station in Aspvreten, Sweden. *Environmental science and technology*, **41**: 6926-6932.

Estin, A. J., Bussey, H. E. (1960). Errors in dielectric measurements due to a sample insertion hole in a cavity. *IRE Transactions on Microwave Theory and Techniques*, **8**: 650 − 653.

Google Maps. (2017). Available: `https://www.google.se/maps/` [2017-05-30]

Hassellöv, M., Readman, J.W., Ranville, J.F., Tiede, K. (2008). Nanoparticle analysis and characterization methodologies in environmental risk assessment of engineered nanoparticles. *Ecotoxicology*, **17**: 344-361.

Hotta, M., Hyashi, M., Lanagan, M. T., Agrawal, D. K., Nagata, K. (2011). Complex permittivity of graphite, carbon black and coal powders in the ranges of X-band frequencies (8.2 to 12.4 GHz) and between 1 and 10 GHz. *ISIJ International*, **51**: 1766-1772.

Huang, X., Wu, S., Du, X. (2016). Gated mesoporous carbon nanoparticles as drug delivery system for stimuli-responsive controlled release. *Carbon*, **101**: 135-142.

Hyung, H., Fortner, J. D., Hughes, J. B., Kim, J. H. (2007). Natural organic matter stabilizes carbon nanotubes in the aqueous phase. *Environmental Science and Technology*, **41**: 179-184.

Iglesias-Groth, S., Cataldo, F. (2010). *Fulleranes: The Hydrogenated Fullerenes*. Springer. Available: Uppsala University E-library [2017-05-28]

Jiang, L., Gao, L., Sun, J. (2003). Production of aqueous colloidal dispersions of carbon nanotubes. *Journal of Colloid and Interface Science*, **260**: 89-94.

Kanpan, P., Khansalee, E., Puangngernmak, N., Chalermwisutkul, S. (2012). TM010 mode cylindrical cavity for complex permittivity measurement of liquid using field analysis technique. *9th International Conference on Electrical Engineering/Electronics, Computer, Telecommunications and Information Technology*.

Karanasiou1, A., Minguillón1, M. C., Vianal, M., Alastueyl, A., Putadu, J. P., Maenhaut, W., Panteliadis, P., Močnik, G., Favez, O., Kuhlbusch, T. A. J. (2015). Thermal-optical analysis for the measurement of elemental carbon (EC) and organic carbon (OC) in ambient air: a literature review. *Atmospheric measurement techniques discussions*, **8**: 9649-9712.

Kroto, H. W., Heath, J. R., O'Brien, S. C., Curl, R. F., Smalley, R. E. (1985). C60: Buckminsterfullerene. *Nature*, **318**: 162 - 163.

Kyotani, T. (2000). Control of pore structure in carbon. *Carbon*, **38**: 269-286.

Law, J., Rennie, R. (2015a). Dielectric. *A Dictionary of Physics*. 7 ed. Oxford University Press. Available: `http://www.oxfordreference.com/view/10.1093/acref/9780198714743.001.0001/acref-9780198714743-e-763` [2017-06-09]

Law, J., Rennie, R. (2015b). Permittivity. *A Dictionary of Physics*. 7 ed. Oxford University Press. Available: `http://www.oxfordreference.com/view/10.1093/acref/9780198714743.001.0001/acref-9780198714743-e-2255` [2017-06-09]

Law, J., Rennie, R. (2015c). Impedance. *A Dictionary of Physics*. 7 ed. Oxford University Press.

Available: `http://www.oxfordreference.com/view/10.1093/acref/9780198714743.001.0001/acref-9780198714743-e-1472` [2017-06-09]

Law, J., Rennie, R. (2015d). Transmittance. *A Dictionary of Physics.* 7 ed. Oxford University Press. Available: `http://www.oxfordreference.com/view/10.1093/acref/9780198714743.001.0001/acref-9780198714743-e-3131` [2017-06-09]

Langa, F., Nierengarten, J. F. (2012). *Fullerenes - Principles and Applications.* 2nd ed. Royal Society of Chemistry. Available: Uppsala University E-Library. [2017-05-27]

Liang, C., Li, Z., Dai, S. (2008). Mesoporous carbon materials: synthesis and modification. *Angwandte Chemie International Edition*, **47**: 3696-3717.

Liu, L., Kong, L. B., Yin, W. Y., Chen, Y., Matitsine, S. (2010). Microwave dielectric properties of carbon nanotube composites. In: Marulanda, J. M., *Carbon nanotubes.* Rijeka, InTech. Chapter 5. Available:
`https://www.intechopen.com/books/carbon-nanotubes/microwave-dielectric-properties-of-carbon-nanotube-composites` [2017-05-27].

Lobato-Morales, H., Corona-Cháves, A., Murthy, D. V. B., Olvera-Cervantes, J. L. (2010). Complex permittivity measurements using cavity perturbation technique with substrate integrated waveguide cavities. *Review of Scientific Instruments*, **81**.

Long, C. M., Nascarella M. A., Valberg, P. A. (2013). Carbon black vs. black carbon and other airborne materials containing elemental carbon: physical and chemical distinctions. *Environmental Pollution*, **181**: 271-286.

Medalia, A. I., Rivin, D. (1982). Particulate carbon and other components of soot and carbon black. *Carbon*, **20**: 481-492.

Miao, H.Y., Liu, J. H., Tsao, C. W., Pan, J. W. (2015). Dielectric property determination of hybrid Al2O3-filled MWCNT buckypaper by the rectangular cavity perturbation technique. *Applied Physics A*, **199**: 211-217.

Mojica M., Alonso J. A., Méndez F. Synthesis of fullerenes. (2013). *Journal of Physical Organic Chemistry*, **26**: 526-539.

Nordling, C., Österman, J. (2011). *Physics Handbook for Science and Engineering*, 8:6th ed., Lund: Studentlitteratur, p. F-5.5.

Nowack, B., Bucheli, T. D. (2007). Occurrence, behavior and effects of nanoparticles in the environment. *Environmental Pollution*, **150**: 5-22.

Obrzut, J., Orloff, N., Kirilov, O. (2014). Non-contact conductance measurement of nanosize object using resonant cavity. *Instrumentation and Measurement Technology Conference (I2MTC) Proceedings*, 2014 IEEE International.

Park, C., Allaby, M. (2017). Organic matter. *A Dictionary of Environment and Conservation.* 3 ed. Oxford University Press. Available: `http://www.oxfordreference.com/view/10.1093/acref/9780191826320.001.0001/acref-9780191826320-e-5697` [2017-06-09]

Pozar, D.M. (2012a). *Microwave engineering.* 4th ed. Hoboken, New Jersey: Wiley, p. 7.

Pozar, D.M. (2012b). *Microwave engineering.* 4th ed. Hoboken, New Jersey: Wiley, p. 10.

Pozar, D.M. (2012c). *Microwave engineering.* 4th ed. Hoboken, New Jersey: Wiley, p. 12.

Pozar, D.M. (2012d). *Microwave engineering.* 4th ed. Hoboken, New Jersey: Wiley, p. 309.

Prasek, J., Drbohalavova, J., Chomoucka, J., Hubalek, J., Jasek, O., Adam, V., Kizek, R. (2011). Methods for carbon nanotubes synthesis - review. *Royal Society of Chemistry*, **21**: 15872-15884.

Qin, F., Brosseau, C. (2012). A review and analysis of microwave absorption in polymer composites filled with carbonaceous particles. *Journal of Applied Physics*, **111**: 061301.

Sarafis, P., Nassiopolou A.G. (2014). Dielectric properties of porous silicon for use as a substrate for the on-chip integration of millimeter-wave devices in the frequency range 140 to 210 GHz. *Nanoscale Research Letters*, **9**: 418.

Schwarz, J. P., Doherty, S. J., Ruggiero, S. T., Tanner, C. E., Perring, A. E., Gao, R. S., Fahey, D. W. (2012). Assessing single particle soot photometer and integrating sphere/integrating sandwich spectrophotometer measurement techniques for quantifying black carbon concentration in snow. *Atmospheric Measurement Techniques*, **5**: 2581-2592.

Schwarz, J. P., Perring, A. E., Markovic, M. Z., Gao, R. S., Ohata, S., Langridge, J., Law, D., McLaughlin, R., Fahey, D. W. (2015). Technique and theoretical approach for quantifying the hygroscopicity of black-carbon-containing aerosol using a single particle soot photometer. *Journal of Aerosol Science*, **81**: 110-126.

Sigma-Aldrich, a. *Fullerene-C60*. Available:
`http://www.sigmaaldrich.com/catalog/product/aldrich/572500?lang=en&region=SE` [2017-05-28]

Sigma-Aldrich, b. *Carbon, mesoporous*. Available:
`http://www.sigmaaldrich.com/catalog/product/aldrich/699624?lang=en&region=SE` [2017-05-28]

Sigma-Aldrich, c. *High Surface Area Graphitized Mesoporous Carbons*. Available: `http://tinyurl.com/yckdf69k` [2017-05-28]

SMHI Öppna Data (2017). Available: `https://opendata-catalog.smhi.se` [2017-05-30]

Taberna, P. L., Simon, P., Fauvarque, J. F. (2003). Electrochemical characteristics and impedance spectroscopy studies of carbon-carbon supercapacitors. *Journal of the Electrochemical Society*, **150**.

US Environmental Protection Agency (US EPA). (2012). *Report to Congress on Black Carbon*. Office of Radiation and Indoor Air, Office of Air Quality Planning and Standards, Office of Atmospheric Programs, Office of Research and Development, Office of Transportation and Air Quality. Washington, DC. EPA-450/R-12-001.

Vanderlei Martins, J., Hobbs, P. V., Weiss, R. E., Artaxo, P. (1998). Sphericity and morphology of smoke particles from biomass burning in Brazil. *Journal of Geophysical Research*, **103**: 32,051-32,057.

Walcarius, A. (2013). Mesoporous materials and electrochemistry. *Royal Society of Chemistry*, **42**: 4098-4140.

Waldron, R. A. (1960). Perturbation theory of resonant cavities. *Proceedings of the IEE – Part C: Monographs*, **107**: 272-274.

Wang, R., Tao, S., Shen, H., Huang, Y., Chen, H., Balkanski, Y., Boucher, O., Ciais, P., Shen, G., Li, W., Zhang, Y., Chen, Y., Lin, N., Su, S., Li, B., Liu, J., Liu, W. (2014). Trend in global black carbon emissions from 1960 to 2007. *Environmental science and technology*, **48**: 6780-6787.

Wang, Y., Huang, J., Zananski, T. J., Hopke, P. K., Holsen, T. M. (2010). Impacts of the

Canadian forest fires on atmospheric mercury and carbonaceous particles in northern New York. *Environmental Science and Technology*, **44**: 8435-8440.

Watson, A.Y., Valberg, P.A. (2001). Carbon Black and Soot: Two Different Substances. *American Industrial Hygiene Association*, **62**: 218-228.

Young, H. D., Freedman, R. A. (2016a). *Sears and Zemansky's University Physics: with Modern Physics*, 14th ed., San Francisco: Addison-Wesley, Pearson Education, p. 789-791.

Young, H. D., Freedman, R. A. (2016b). *Sears and Zemansky's University Physics with Modern Physics*. 14th ed. San Francisco: Addison-Wesley, Pearson Education, p. 793-795.

Yttri, K. E., Lund Myhre, C., Eckhardt, S., Fiebig, M., Dye, C., Hirdman, D:, Strom, J., Klimont, Z. (2014). Quantifying black carbon from biomass burning by means of levoglucosan - A one-year time series at the Arctic observatory Zeppelin. *Atmospheric Chemistry and Physics*, **14**: 6421-6442.

UNPUBLISHED MATERIAL

Olsson, J. (2017). *Impedansanalys.* Unpublished material. Professor at Department of Engineering Sciences, Solid State Electronics, Uppsala University. Uppsala: Uppsala University.

Ström, J. (2017). *Calibration graph for NIST and chimney soot.* Unpublished material. Professor at Department of Analytical Chemistry and Environmental Science, Stockholm University. Stockholm: Stockholm University.

APPENDIX

This section contains Matlab scripts, figures and tables not shown in the report.

A   VISUAL FILTER ARCHIVE

A selection of the visual filter archive including the whole MWC filter series (six filters where number 1 has the highest carbon loading) and the filters from the snow samples collected in Arvidsjaur. The NCS greyscale are included in all pictures for easier comparison.
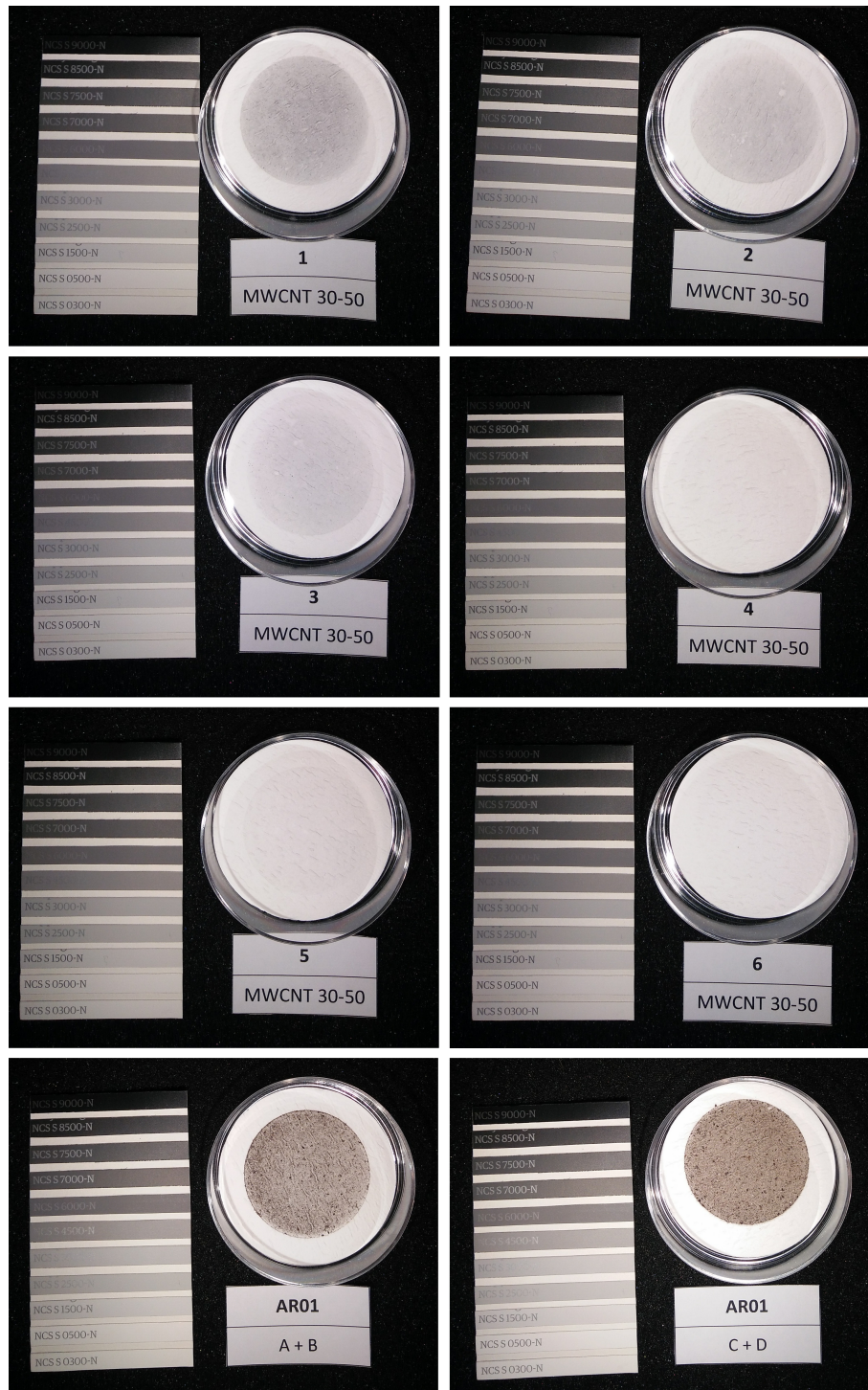
Figure 16: *Pictures of the MWC filters and the filters from snow samples collected in Arvidsjaur with the NCS greyscale for comparison.*

B   PERMITTIVITY CALCULATIONS - MATLAB SCRIPT

The following Matlab script was made to load all the data from the impedance analyzer into the Matlab workspace and calculate the relative permittivity of each filter.

```matlab
files  = dir( '*.txt' ) ; %Find all files ending with .txt in the
    current directory
nFiles = length( files ) ; %Store the amount of files

 for i = 1 : nFiles %Run the same amount of times as there are files in
     folder
     filename = files(i).name; %Extract the exact filename
     load(filename) %Then load that exact file into the matlab
         workspace
 end
 n = 6; %Number of samples per carbon type

%figure
count = 1; %Start from the first , file which contains impedance data
 for k = 1 : nFiles/n %Run this loop for every loading (usually 6 times
     )
     for p = 1:3 %Run this three times to calculate the average
         impedance over the three measuring spots on each filter
     filename = files(count).name(1:end-4);
     count = count+2; %Every other file contains impedance data , skip
         the files containing phase data
     x = eval(filename);
     y(:,p) = x(:,4);
     end
     imp(:,k) = mean(y'); %Calculates the average value for the three
         measuring points

 end
count = 2; %Start from the first phase file
loading = linspace(1,nFiles/n,nFiles/n);

Conc = [1000 500 250 100 50 25]; %Insert the concentrations i[U+FFFD]g L
Vol = 0.25; % Insert the volume of each suspension in L
BC_mass = Conc.*Vol; % Calculate the mass of carbon in suspension
FilterArea = 0.000962; % The area of the filter containing carbonaceous
     particles
BC_surf_dens = BC_mass./FilterArea; %Calculate surface density on BC
    filters i[U+FFFD]g m^2
surf_dens = BC_surf_dens*10^-6; % Calculate surface density in g / m^2

 for k = 1 : nFiles/n
     for p = 1:3 %Run this three times to calculate the average phase
         over the three measuring spots on each filter
     filename = files(count).name(1:end-4);
     count = count+2;  %Every other file contains phase data , skip the
         files containing impedance data
     x = eval(filename); %Extract the name of file in workspace and
         store in x
     y(:,p) = x(:,4);%Extract the phase of the current measuring
         position on filter
     end
```

```matlab
39          fas (:,k) = mean(y'); %Calculates the average phase value for the
                three measuring points
40      end
41      %Extracting the frequency stored at location 103(Corresponding to
            0.915GHz)
42      nyfas = fas(103,1:end);%Do this for both phase
43      nyimp = imp(103,1:end);%and frequency
44
45  d = 0.1/1000; %Thickness of filter [meter]
46  A = 3.84845*10^-5;%Area of the probe [meter]
47
48  %Calculate the parallel capacitance
49      for m = 1:nFiles/n %For all the different loadings
50          Cp(m) = -((sind(nyfas(m))*nyimp(m)))/(2*pi*x(103,1)*nyimp(m)^2);
51      end
52
53  %Insert blan kvalues as comparison
54  blank_values = [[0.344639111571898 0.368704131483751 0.376537449775331
        0.365074802299770]];
55  %Create a vector containing only average blank values
56  blank_avg = [mean(blank_values) mean(blank_values) mean(blank_values)
        mean(blank_values)];
57  %Create x-values to fit this vector into plot
58  blank_x = linspace(min(surf_dens),max(surf_dens),4);
59  varepsilon = Cp.*(d/A); %Calculate the permittivity of the filters
60
61  varepsilon0 = 8.854*10^-12;%And with the use of the permittivity of
        vacuum [F/m]
62  varepsilonR = varepsilon./varepsilon0;%Calculate the relative
        permittivity of the filters
63  figure
64  hold on
65  plot(surf_dens,varepsilonR) %Plot surface density
66  plot(blank_x,blank_avg,'r') %And the blanks
67  legend('Soot','Blank')
68  scatter(surf_dens,varepsilonR,80,'b')
69  xlabel('Surface density [g/m^2]','FontSize',14)
70  ylabel('Relative permittivity','FontSize',14)
```

C   FREQUENCY SHIFT CALCULATIONS
- MATLAB SCRIPT

The following Matlab script was made to calculate frequency shifts for all standards using data from the waveguide measurements.

```matlab
close all
clear all
load('cavityworkspace20170517.mat') %Load the data from the resonant
    cavity measurements
freq = mpc11.Frequencies; %Store the vector containing measured
    frequencies

Conc = [1000*10^-6 500*10^-6 250*10^-6 100*10^-6 50*10^-6 25*10^-6]; %
    Store the concentrations [g/L]
Vol = 0.25; %Store the original suspension volume filtered through the
    filters [L]
BC_mass = Conc.*Vol; %Calculate the mass of the particles on each
    filter [g]
FilterArea = 0.000962; %Store the area of the filter containing
    particles [m^2]
BC_surf_dens = BC_mass./FilterArea; %Calculate the surface density on
    filters in g / m^2
konc = BC_surf_dens; %Store these under the name 'konc'


full61 = rfparam(full61,2,1); %Extract the complex data from the s-
    parameter file of the filter with lowest concentration
full62 = rfparam(full62,2,1); %For all measurements
full6 = (full61+full62)./2; %Calculate the average complex data from
    the measurements
full6_mag = abs(full61(401)); %Calculate the amplitude at 12.15 GHz (
    location 401 in vector)
full6_db = 20*log10(full6_mag); %Transform into decibels
uplim = full6_db-(full6_db/100); %Set limits to how much the amplitude
    may vary when searching
lowlim = full6_db+(full6_db/100); %for it in the other filters

full51 = rfparam(full51,2,1); %Extract the complex data from the s-
    parameter file of the remaining filters
full52 = rfparam(full52,2,1);
full5 = (full51+full52)./2;
full51_mag_db = 20*log10(abs(full51));
full51_mag_db = 20*log10(abs(full52));
full5_mag_db = (full51_mag_db+full51_mag_db)./2;
full5_loc = find(full5_mag_db>lowlim & full5_mag_db<uplim); %Find the
    amplitude within the limits
full5_loca = find(full5_loc >360);
full5_loc = full5_loc(full5_loca(1)); %If there are several values,
    extract the first one in vector
full5_freq = freq(full5_loc); %Store it as the frequency corresponding
    to the examined filter

full41 = rfparam(full41,2,1); %Do this for all the remaining filters of
    each carbon types
full42 = rfparam(full42,2,1);
full4 = (full41+full42)./2;
full41_mag_db = 20*log10(abs(full41));
```

```matlab
37  full41_mag_db = 20*log10(abs(full42));
38  full4_mag_db = (full41_mag_db+full41_mag_db)./2;
39  full4_loc = find(full4_mag_db>lowlim & full4_mag_db<uplim);
40  full4_loca = find(full4_loc >360);
41  full4_loc = full4_loc(full4_loca(1));
42  full4_freq = freq(full4_loc);
43
44  full31 = rfparam(full31,2,1);
45  full32 = rfparam(full32,2,1);
46  full3 = (full31+full32)./2;
47  full31_mag_db = 20*log10(abs(full31));
48  full31_mag_db = 20*log10(abs(full32));
49  full3_mag_db = (full31_mag_db+full31_mag_db)./2;
50  full3_loc = find(full3_mag_db>lowlim & full3_mag_db<uplim);
51  full3_loca = find(full3_loc >360);
52  full3_loc = full3_loc(full3_loca(1));
53  full3_freq = freq(full3_loc);
54
55  full21 = rfparam(full21,2,1);
56  full22 = rfparam(full22,2,1);
57  full2 = (full21+full22)./2;
58  full21_mag_db = 20*log10(abs(full21));
59  full21_mag_db = 20*log10(abs(full22));
60  full2_mag_db = (full21_mag_db+full21_mag_db)./2;
61  full2_loc = find(full2_mag_db>lowlim & full2_mag_db<uplim);
62  full2_loca = find(full2_loc >360);
63  full2_loc = full2_loc(full2_loca(1));
64  full2_freq = freq(full2_loc);
65
66  full11 = rfparam(full11,2,1); %Until data for all of the filters have
        been loaded into matlab
67  full12 = rfparam(full12,2,1);
68  full1 = (full11+full12)./2;
69  full11_mag_db = 20*log10(abs(full11));
70  full11_mag_db = 20*log10(abs(full12));
71  full1_mag_db = (full11_mag_db+full11_mag_db)./2;
72  full1_loc = find(full1_mag_db>lowlim & full1_mag_db<uplim);
73  full1_loca = find(full1_loc >360);
74  full1_loc = full1_loc(full1_loca(1));
75  full1_freq = freq(full1_loc);
76
77  full_frequencies = [full1_freq full2_freq full3_freq full4_freq
        full5_freq freq(401)]; %Store all frequencies
78  [fullF fullF_I] = sort(full_frequencies) %Sort them from small to large
79  fullF = [0 fullF(2)-fullF(1) fullF(3)-fullF(1) fullF(4)-fullF(1) fullF
        (5)-fullF(1) fullF(6)-fullF(1)]*10^-6; %Normalize against the
        smallest
80  konc_full = konc(fullF_I); %And make sure the surface densities
        correspond to the correct frequency
81
82  figure %Open up a new figure
83  scatter(konc_full,fullF,'filled') %Plot these in a scatter diagram
84  ylabel('Frequency shift [MHz]','FontSize',14)
85  xlabel('Surface density [g/m^2]','FontSize',14)
86  legend('Fullerene')
87  a = get(gca,'XTickLabel');
88  set(gca,'XTickLabel',a,'FontName','Arial','fontsize',14)
```

D   CALIBRATION CURVE FOR NIST SOOT

In a personal meeting with J. Ström (2017) at Stockholms University a relationship between τ and EC density was discussed, discovered from analyses of two types of soot. The relationship is linear and is represented by the slope of the lines seen in Figure 17. The two different soots used were a collected chimney soot and a standardized soot from the U.S. National Institute of Standards and Technology (NIST). The EC density shown in Figure 17 was obtained from independent measurements, using a Sunset Laboratory OC-EC analyzer on filters prepared with a similar procedure as in this study. The corresponding values for τ were obtained through PSAP measurements, also using the same instrumentation as in this study (Ström, 2017). Using Equation 19, the density of EC and soot on our filters could be approximated.

$$ECdensity = \frac{\tau}{slope} \tag{19}$$
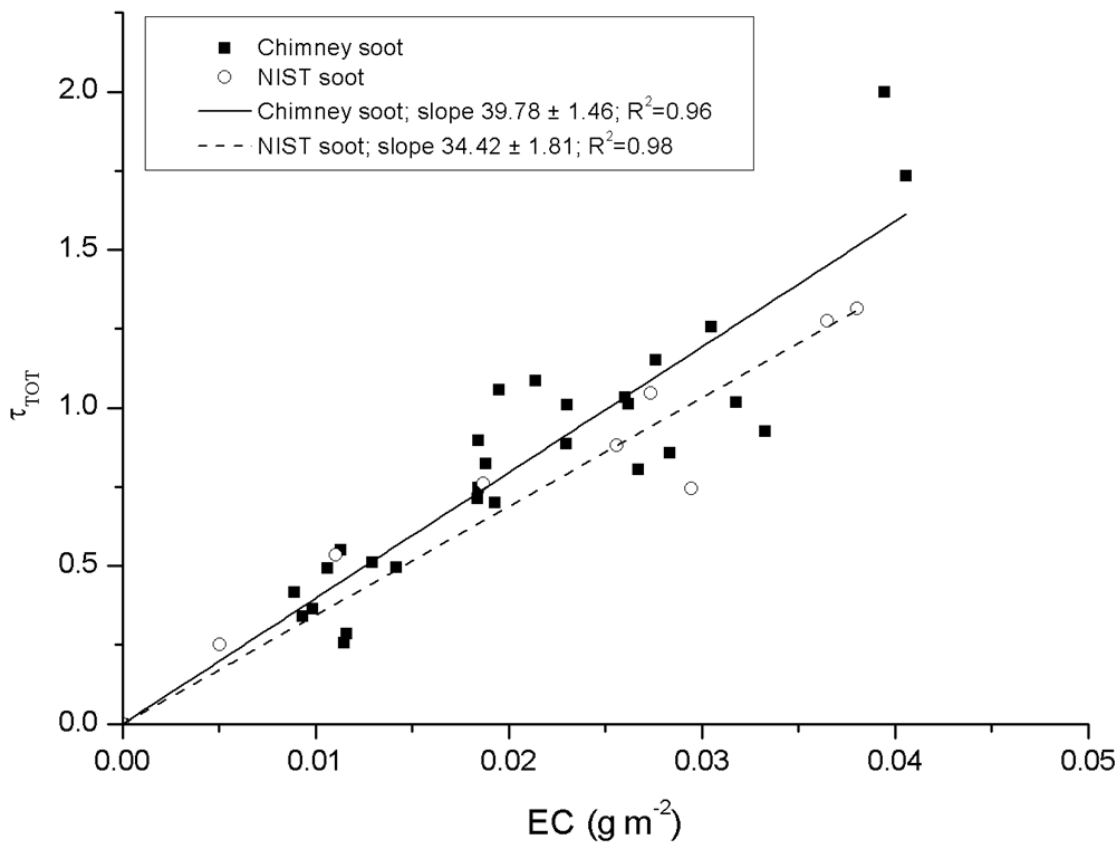
Figure 17: *Showing the relationship between τ and EC density for two different soot types, chimney soot and standardized soot from NIST. Displayed with kind permission from Johan Ström (Ström, 2017).*

E MAXWELL GARNETT FORMULA - MATLAB SCRIPT

The following script was used to calculate the effective relative permittivity in Matlab.

```matlab
% This simple MATLAB calculator computes the effective dielectric
% constant of a mixture of an inclusion material in a base medium
% according to the Maxwell Garnett theory as introduced in:
% http://en.wikipedia.org/wiki/Effective_Medium_Approximations
% INPUTS:
%   eps_base: dielectric constant of base material;
%   eps_incl: dielectric constant of inclusion material;
%   vol_incl: volume portion of inclusion material;
% OUTPUT:
%   eps_mean: effective dielectric constant of the mixture.

function [eps_mean] = MaxwellGarnettFormula(eps_base, eps_incl,
    vol_incl)
small_number_cutoff = 1e-6;
% if vol_incl < 0 || vol_incl > 1
%     disp(['WARNING: volume portion of inclusion material is out of
    range!']);
% end
factor_up = 2*(1-vol_incl)*eps_base+(1+2*vol_incl)*eps_incl;
factor_down = (2+vol_incl)*eps_base+(1-vol_incl)*eps_incl;

if abs(factor_down) < small_number_cutoff
    disp(['WARNING: the effective medium is singular!']);
    eps_mean = 0;
else
    eps_mean = eps_base*factor_up/factor_down;
end
```

F UV/VIS SPECTROPHOTOMETRY RESULTS - AQUEOUS SUSPENSIONS

The relation of absorbance and concentration for MPC, fullerene C_{60} and MWCNT.
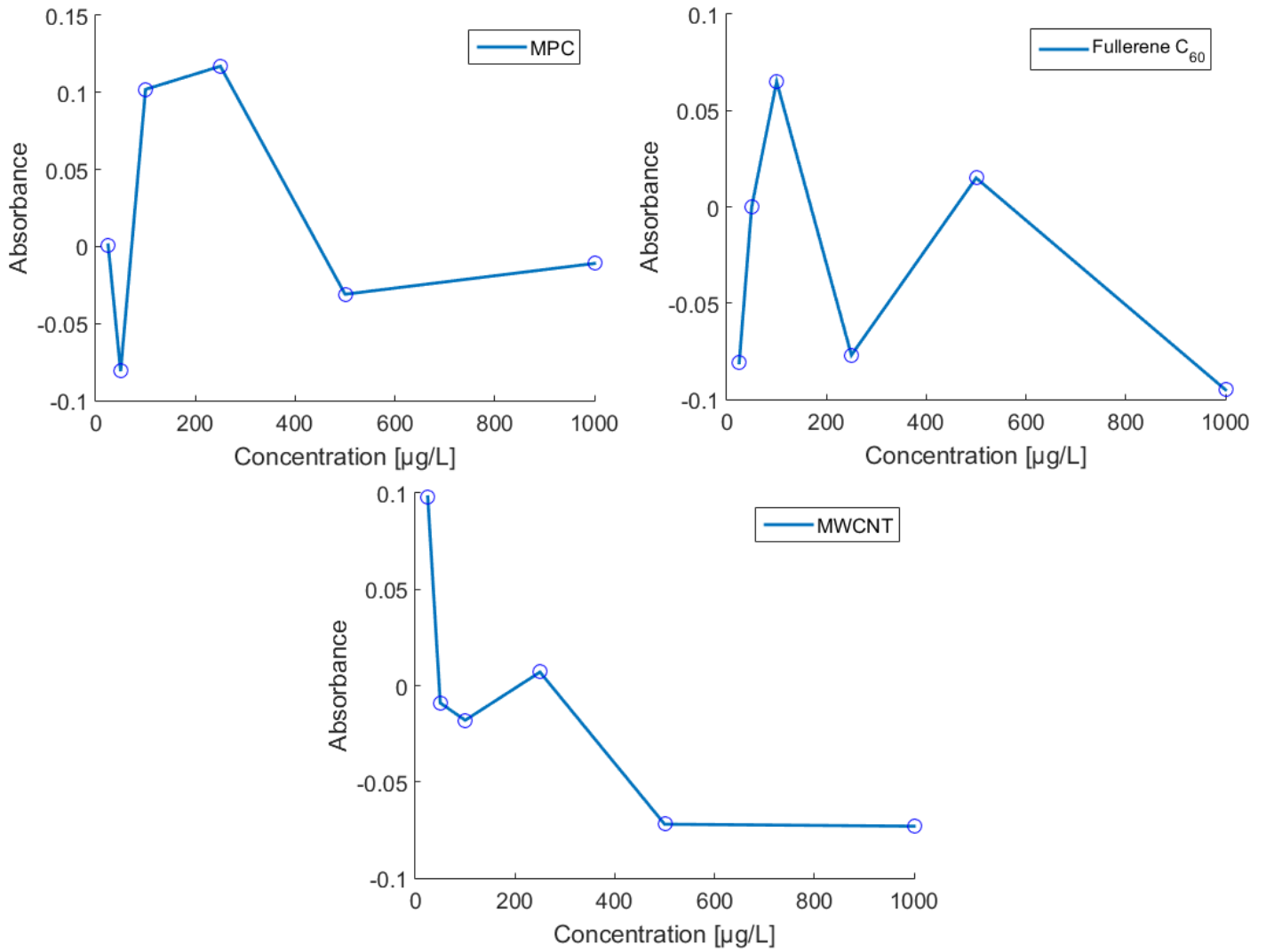
Figure 18: *The absorbance of the different standard suspensions, except for soot. Each circle represents a filter.*

G UV/VIS SPECTROPHOTOMETRY RESULTS - ON FILTERS

The relation of transmittiance and surface density for MWCNT and fullerene C_{60} at 325 nm.
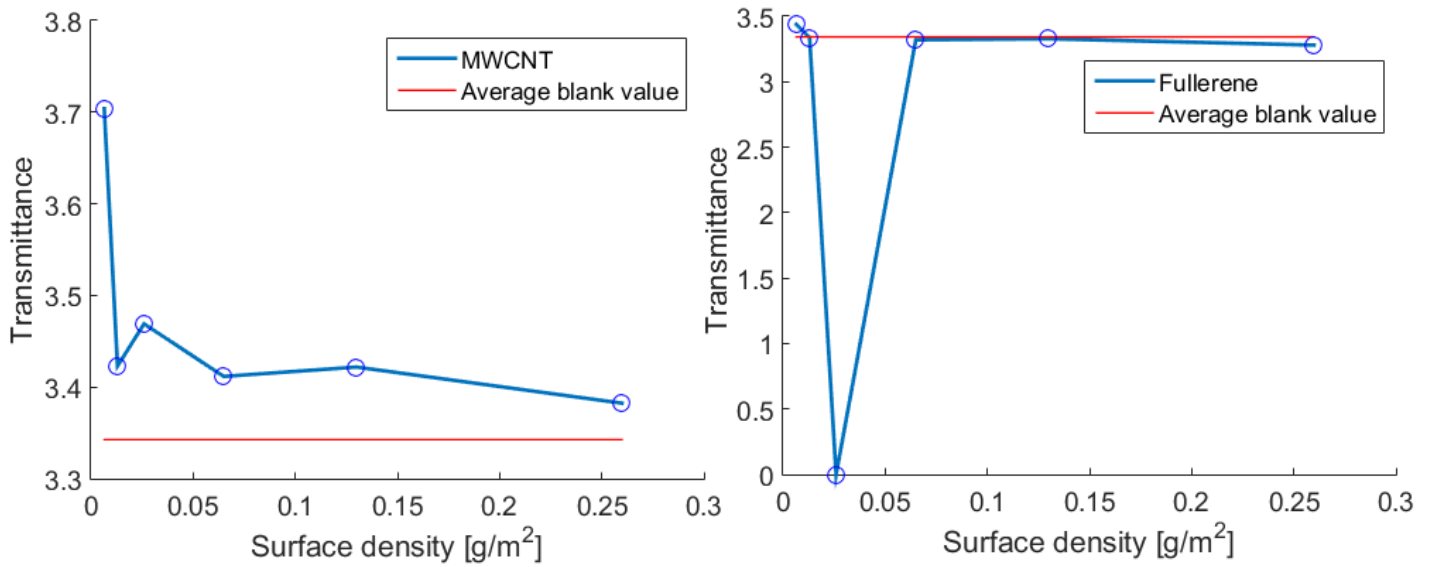
Figure 19: *The transmittance of MWCNT and fullerene C_{60}. Each circle represents a filter.*

H CALIBRATION SLOPES
- FROM LINEAR REGRESSION

Linear regression between tau and the surface densities of the filters. These values were used to estimate the surface densities on the snow sample filters.

Table 5: *Slopes for each standard carbon type calculated with linear regression of the graphs shown in Figure 10*

	MWCNT	Fullerene C_{60}	MPC	Soot
Slope [m^2/g]	6.53	4.64	1.99	3.93

I VALIDATAION OF STANDARD SAMPLE CONCENTRATIONS

Carbon particle concentrations of suspensions where the calibrations curves for MPC, MWCNT and fullerene C_{60} have been used.
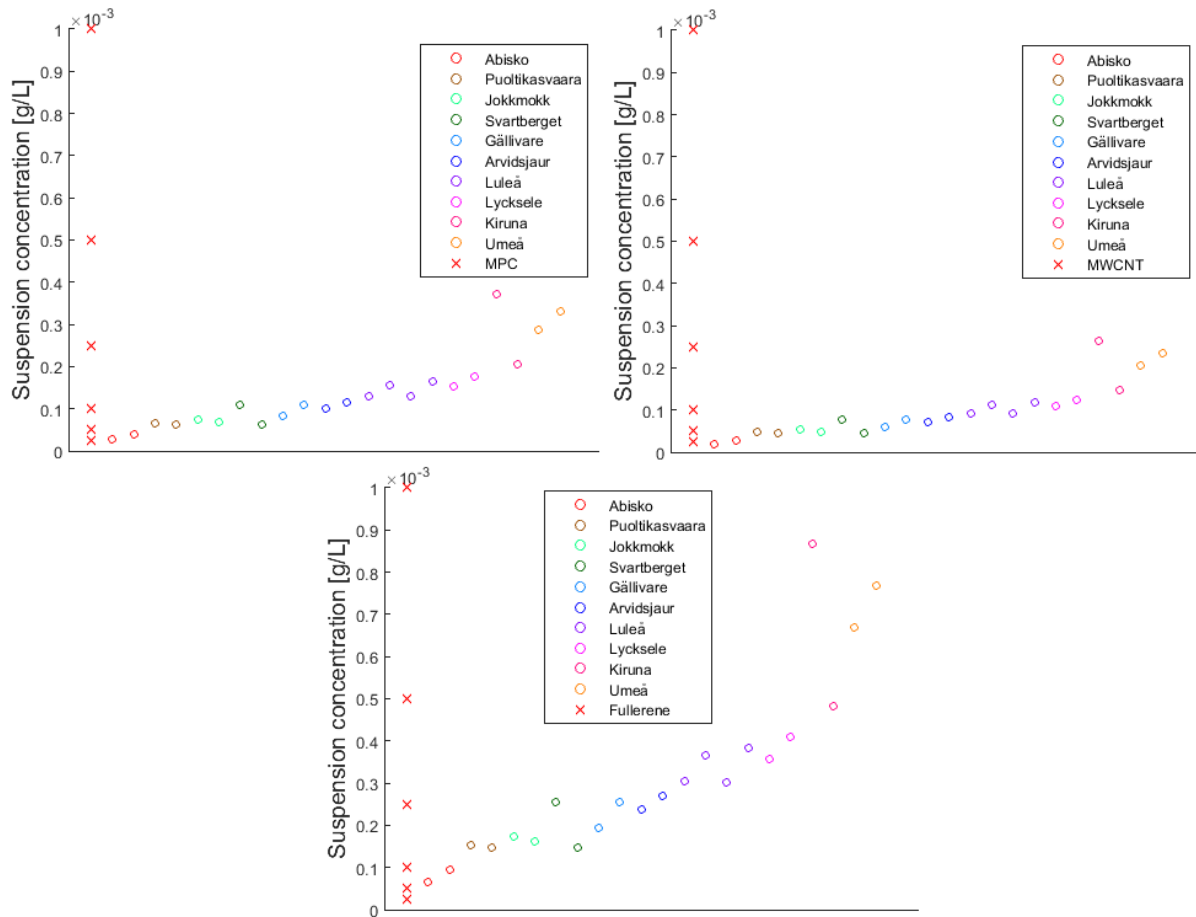
Figure 20: *The estimated concentrations of BC in the snow samples using the calibration curve for MPC, MWCNT and fullerene C_{60} respectively.*

J SNOW SAMPLE LOCATIONS AND ASSEMBLED SITE INFORMATION

Table 6 gives an explanation of the numbered sites, according to Figure 5, with a short description of the sampling area and conditions.

Table 6: *Sample locations with short descriptions of the sampling area. The coordinates are according to the geographic coordinate system*

Nr	Place	Coordinates	Date	Short description of sampling area	Average total snow depth [cm]	Number of snow layers	Average temp. in total snow layer [°C]
1	Umeå	N63°52.138' E20°24.994'	3 April 2017	Very close to thermal power plant and road	49	4	0
2	Umeå	N63°52.137' E20°25.204'	3 April 2017	Forest clearing close to thermal power plant and snow scooter tracks	37	3	-0.6
3	Luleå	N65°37.275' E22°10.252'	3 April 2017	Residential area with snow scooter tracks close by	69	4	-0.8
4	Gällivare	N67°09.186' E20°43.378'	4 April 2017	Forest clearing close to mining service factory and snow scooter tracks	99	3	-3.4
5	Puoltikas-vaara	N67°26.294' E21°06.075'	6 April 2017	Clearing in rural environment	70	3	-0.7
6	Kiruna	N67°49.991' E20°15.354'	4 April 2017	Clearing close to residential area and snow scooter tracks	66	2	-2.5
7	Abisko	N68°21.818' E18°45.571'	5 April 2017	Clearing in remote area	73	4	-0.6
8	Jokkmokk	N66°36.340' E19°46.758'	6 April 2017	Clearing in a reindeer pen	68	2	-0.4
9	Arvidsjaur	N65°32.427' E19°13.342'	6 April 2017	Clearing close to snow scooter trail	64	3	0
10	Lycksele	N64°36.248' E18°43.652'	7 April 2017	Clearing close to scooter and reindeer trail	64	3	-1.1
11	Svartberget	N64°15.354' E19°47.040'	7 April 2017	Clearing in remote area	78	5	-1.9